frontiers | Frontiers in Immunology

TYPE Original Research
PUBLISHED 16 September 2024
DOI 10.3389/fimmu.2024.1432334

OPEN ACCESS

EDITED BY
Changwan Hong,
Pusan National University, Republic of Korea

REVIEWED BY
Carla Guenther,
Osaka University, Japan
Kristi Warren,
The University of Utah, United States

*CORRESPONDENCE
Aaron D. Schwab
aaron.schwab@unmc.edu

RECEIVED 13 May 2024
ACCEPTED 22 August 2024
PUBLISHED 16 September 2024

CITATION
Schwab AD, Nelson AJ, Gleason AM, Schanze OW, Wyatt TA, Shinde DD, Xiao P, Thomas VC, Guda C, Bailey KL, Kielian T, Thiele GM and Poole JA (2024) Aconitate decarboxylase 1 mediates the acute airway inflammatory response to environmental exposures.
Front. Immunol. 15:1432334.
doi: 10.3389/fimmu.2024.1432334

Aconitate decarboxylase 1 mediates the acute airway inflammatory response to environmental exposures

Aaron D. Schwab[1]*, Amy J. Nelson[1], Angela M. Gleason[1], Oliver W. Schanze[1], Todd A. Wyatt[2,3,4], Dhananjay D. Shinde[5], Peng Xiao[6], Vinai C. Thomas[5], Chittibabu Guda[6], Kristina L. Bailey[2,3], Tammy Kielian[5], Geoffrey M. Thiele[3,7] and Jill A. Poole[1]

[1]Division of Allergy & Immunology, Department of Internal Medicine, College of Medicine, University of Nebraska Medical Center, Omaha, NE, United States, [2]Division of Pulmonary, Critical Care and Sleep Medicine, Department of Internal Medicine, College of Medicine, University of Nebraska Medical Center, Omaha, NE, United States, [3]Veterans Affairs Nebraska-Western Iowa Health Care System, Research Service, Omaha, NE, United States, [4]Department of Environmental, Agricultural and Occupational Health, College of Public Health, University of Nebraska Medical Center, Omaha, NE, United States, [5]Department of Pathology, Microbiology, and Immunology, University of Nebraska Medical Center, Omaha, NE, United States, [6]Department of Genetics, Cell Biology and Anatomy, University of Nebraska Medical Center, Omaha, NE, United States, [7]Division of Rheumatology & Immunology, Department of Internal Medicine, College of Medicine, University of Nebraska Medical Center, Omaha, NE, United States

Background: Environmental lipopolysaccharide (LPS) and microbial component-enriched organic dusts cause significant lung disease. These environmental exposures induce the recruitment and activation of distinct lung monocyte/macrophage subpopulations involved in disease pathogenesis. Aconitate decarboxylase 1 (*Acod1*) was one of the most upregulated genes following LPS (vs. saline) exposure of murine whole lungs with transcriptomic profiling of sorted lung monocyte/macrophage subpopulations also highlighting its significance. Given monocyte/macrophage activation can be tightly linked to metabolism, the objective of these studies was to determine the role of the immunometabolic regulator ACOD1 in environmental exposure-induced lung inflammation.

Methods: Wild-type (WT) mice were intratracheally (i.t.) instilled with 10 µg of LPS or saline. Whole lungs were profiled using bulk RNA sequencing or sorted to isolate monocyte/macrophage subpopulations. Sorted subpopulations were then characterized transcriptomically using a NanoString innate immunity multiplex array 48 h post-exposure. Next, WT and *Acod1*$^{-/-}$ mice were instilled with LPS, 25% organic dust extract (ODE), or saline, whereupon serum, bronchoalveolar lavage fluid (BALF), and lung tissues were collected. BALF metabolites of the tricarboxylic acid (TCA) cycle were quantified by mass spectrometry. Cytokines/chemokines and tissue remodeling mediators were quantitated by ELISA. Lung immune cells were characterized by flow cytometry. Invasive lung function testing was performed 3 h post-LPS with WT and *Acod1*$^{-/-}$ mice.

10.3389/fimmu.2024.1432334

Results: *Acod1*$^{-/-}$ mice treated with LPS demonstrated decreased BALF levels of itaconate, TCA cycle reprogramming, decreased BALF neutrophils, increased lung CD4^{+} T cells, decreased BALF and lung levels of TNF-α, and decreased BALF CXCL1 compared to WT animals. In comparison, *Acod1*$^{-/-}$ mice treated with ODE demonstrated decreased serum pentraxin-2, BALF levels of itaconate, lung total cell, neutrophil, monocyte, and B-cell infiltrates with decreased BALF levels of TNF-α and IL-6 and decreased lung CXCL1 vs. WT animals. Mediators of tissue remodeling (TIMP1, MMP-8, MMP-9) were also decreased in the LPS-exposed *Acod1*$^{-/-}$ mice, with MMP-9 also reduced in ODE-exposed *Acod1*$^{-/-}$ mice. Lung function assessments demonstrated a blunted response to LPS-induced airway hyperresponsiveness in *Acod1*$^{-/-}$ animals.

Conclusion: *Acod1* is robustly upregulated in the lungs following LPS exposure and encodes a key immunometabolic regulator. ACOD1 mediates the proinflammatory response to acute inhaled environmental LPS and organic dust exposure-induced lung inflammation.

KEYWORDS

ACOD1, organic dust, endotoxin, environmental health, immunometabolism, macrophages, inhalation

Introduction

Of the 12.6 million deaths that result from unhealthy environments every year, 8.2 million are caused by non-communicable diseases mostly originating from inhaled exposure (1). Industrial and agricultural intensification synergistically elevates worker and non-worker risk for adverse respiratory health outcomes (2–5). Biologic material use in agricultural, waste treatment, recycling, and food production work settings elevates the risk of inhaling harmful bioaerosols, particularly organic dust (6, 7). Organic dusts are complex, heterogeneous collections of particle-associated bacterial and fungal components that provoke lung inflammatory responses (8). An immunogenic component of many disease-causing environmental dusts is lipopolysaccharide (LPS) or endotoxin, a membrane component of gram-negative bacteria (9, 10). Despite advances in identifying respirable hazards and understanding the key signaling pathways involved in mediating the lung inflammatory response, there remains a paucity of knowledge and efficacious therapeutic options to accelerate recovery and prevent disease progression.

Recruited and activated lung monocyte/macrophage subpopulations induced by environmentally sourced organic dust extract (ODE) and LPS have been identified as central mediators of tissue damage, inflammation, and fibrosis as well as resolution and recovery processes (11–19). Specifically, lung monocyte/macrophage subpopulations have been implicated in driving the transition from acute lung inflammation to tissue recovery, with the initiation of prefibrotic processes having potential long-term, adverse health outcomes (11, 20, 21). Whereas the interplay between lung monocyte/macrophage function and metabolic plasticity is appreciated in pulmonary infection, sepsis, and chronic lung disease, its role in inhaled environmental exposure-induced lung injury is unknown (22–26). As monocyte/macrophage recruitment and activation is tightly linked to cellular metabolism, studying the immunomodulatory role of metabolic enzymes and their bioactive metabolites represents a new avenue for mechanistic characterization and potential therapy development (27).

An emerging immunometabolic regulator of activated monocytes/macrophages is aconitate decarboxylase 1 (ACOD1). ACOD1 is a multifunctional regulator of infection and inflammation responsible for itaconate metabolism and is found predominately in the mitochondria (28, 29). The biological implications of ACOD1 are becoming increasingly nuanced as it plays context-dependent roles in the regulation of both pro- and anti-inflammatory responses after induction by inflammatory stimuli (30). In various inflammatory and infectious contexts, *Acod1*-deficient mice have exhibited more robust proinflammatory cytokine burst, aberrant neutrophil infiltration, and worsened survival (29). Conversely, ACOD1 induction can promote virus replication, exacerbate ROS-mediated tissue damage, induce immune paralysis, and cause ferroptosis-mediated cell death (31). In the context of lung disease, itaconate has been shown to mitigate pulmonary fibrosis severity, interferon responses in influenza A infection, and pulmonary *Brucella* proliferation and infection (32–34). ACOD1/itaconate deficiency has also been shown to exacerbate endotoxemia-induced acute lung injury via the inhibition of autophagy (35). Additionally, *Acod1* deletion augmented urban dust particulate matter (PM)-induced macrophage production of

IL-6 and IL-1β although mouse lung inflammation following an *in-vivo* PM exposure was not affected by ACOD1 (36).

We sought to characterize transcriptomic changes at the whole lung and monocyte/macrophage subpopulation levels to identify critical mediators of exposure-induced lung inflammation. These transcriptomic investigations demonstrated robust *Acod1* upregulation, prompting us to determine the role of ACOD1 in mediating the lung inflammatory response and resolution processes following inhaled, environmentally relevant inflammatory exposures. We used *Acod1*-deficient (knockout) mice to characterize the relative changes in inflammatory responses, carbohydrate metabolism, pathology, tissue repair, and airway hyperresponsiveness (AHR) that occur in the absence of ACOD1. Elucidation of the role of ACOD1 in this model may inform novel therapeutic strategies for environmental exposure-induced lung disease.

Materials and methods

Environmental exposure agents: LPS and ODE

LPS from gram-negative *Escherichia coli* (O55:B5; Sigma, St. Louis, MO) and an aqueous ODE prepared from swine confinement feeding facilities (17) served as the two inhalant exposure agents. Briefly, settled surface dust (1 g) was incubated in sterile Hank's Balanced Salt Solution (10 mL; Mediatech, Manassas, VA) for 1 h and centrifuged for 30 min at 2,850×*g* twice, with the final supernatant filter-sterilized (0.22 um) to remove microorganisms and coarse particles. Stock ODE was batch prepared and stored at −20°C; aliquots were diluted for each experiment to a final concentration (vol/vol) of 25% in sterile phosphate-buffered saline (PBS, pH 7.4; diluent). The rationale for the use of LPS is that it is commercially available and elicits dose-dependent, reproducible proinflammatory lung responses in humans and rodents that could be translated to various environmental exposures. Agricultural ODE represents a "real-life" complex organic dust exposure. Endotoxin concentrations were determined using the limulus amebocyte lysate assay (Lonza, Walkersville, MD). Endotoxin levels averaged 1.308–2.616 µg (~10–50 EU) for 25% ODE. Prior mass spectrometry studies of ODE have revealed significant amounts of muramic acid (peptidoglycan marker) and 3-hydroxy fatty acids (endotoxin marker), but not ergosterol (fungi marker) as compared to house dust (17).

Mean or median concentrations of endotoxin in ambient air generally fall in the range of 0.006–5.7 EU/m^3 (2). Polluted urban environments, however, can achieve endotoxin concentrations as high as 75 EU/m^3 (37). Agricultural practices elevate endotoxin concentrations where concentrated animal feeding operations (CAFOs) can have endotoxin concentrations ranging from <1 to 4,153 EU/m^3 with upwind ambient concentrations averaging 22.8 EU/m^3 and downwind ambient concentrations averaging 65.3 EU/m^3 (38). Our 10-µg LPS dose is used to model an acute, high-concentration exposure to a bacterial component-enriched environment, whereas our ODE exposure is intended to model a complex exposure to organic dust comprised of an endotoxin concentration comparable to real-life exposure.

Animal exposure model

For transcriptomic investigations, C57BL/6 mice (between 6 and 8 weeks of age) were purchased from The Jackson Laboratory (Bar Harbor, ME), randomized upon arrival, and allowed to acclimate for 1 week prior to initiation of experiments (note: the authors A.J.N. and A.G. and facility staff were aware of the randomization, whereas all the other authors were blinded). Male mice were utilized for all transcriptomic studies because we have previously demonstrated that female mice were less susceptible to inflammatory agent inhalation-induced airway and systemic inflammatory effects (39). Airway inflammation was induced using a singular intratracheal instillation whereby mice were lightly sedated under the continual flow of 1.5% isoflurane (VetOne, Boise, ID) and received treatment with either 50 µL of sterile saline or 10 µg of LPS.

For studies exploring the role of ACOD1 in environmental exposure-induced lung inflammation, C57BL/NJ6 (WT) and C57BL/6NJ-*Acod1*$^{em1(IMPC)J}$/J (*Acod1*$^{-/-}$) mice between 6 and 8 weeks of age were purchased from The Jackson Laboratory (Bar Harbor, ME). In the latter strain (#029340; RRID: IMSR_JAX:029340), the aconitate decarboxylase 1 (*Acod1*) encoding gene was knocked out by means of CRISPR technology [Knockout Mouse Phenotyping Program (KOMP^2) at The Jackson Laboratory]. The *Acod1*$^{-/-}$ mice have normal development without adverse phenotypic differences relative to WT mice. Both male and female mice were utilized for these studies comparing WT and *Acod1*$^{-/-}$ animal responses to environmental exposures to capture potential sex-mediated differences. Mice were lightly sedated under isoflurane (VetOne, Boise, ID) and received one treatment with 50 µL of LPS (10 µg) or ODE (25%) (8). Control (CXN) mice represent WT (C57BL/NJ6) mice intratracheally (i.t.) instilled with sterile saline. An intubation laryngoscope (Harvard Apparatus, Holliston, MA) enabled tracheal visualization and access to the intratracheal instillation technique. Weights were recorded daily, and all animals were euthanized 48 h after the acute environmental agent exposure by isoflurane followed by exsanguination (right axillary blood collection). Our previous work identified peak monocyte/macrophage lung recruitment and activation at 48 h (2 days) post-LPS exposure with corresponding elevations in inflammatory markers and resolution of most inflammatory indices by 1 week (15). Similar findings were also reported with organic dust extract exposure (18). Thus, to adequately capture differences in cellular recruitment and inflammatory mediator prevalence, we utilized this 2-day timepoint. No respiratory distress, signs of stress, or significant weight loss (defined as >20%) was observed throughout this period.

Fluorescence-activated cell sorting of monocyte/macrophage subpopulations

In three independent studies with two to four mice pooled per treatment group (LPS or saline, respectively) and following removal

of blood from pulmonary vasculature, lungs were inflated with 1 mL of digestion solution/mouse containing 0.5 mg/mL of Liberase™ (Millipore Sigma, St. Louis, MO) and 235.5 U/mL of DNAse I in Hank's Balanced Salt Solution (pH = 7.2). Lung cells were dissociated with a gentleMACS dissociator (Miltenyi Biotech, Auburn, CA) and incubated for 15 min at 37°C in a shaking incubator. Digestion solution activity was neutralized with FA3 buffer (10 mM of HEPES, 2 mM of EDTA, 1% FBS in PBS). The single-cell lung suspensions were incubated with CD16/32 (Fc Block, Biolegend, San Diego, CA) to minimize non-specific antibody staining. Next, cells were stained with monoclonal antibodies (mAbs) directed against rat anti-mouse CD45 (clone 30-F11; BD Biosciences, Franklin Lakes, NJ), Ly6C (clone AL-21, BD Biosciences), Ly6G (clone 1A8, BD Biosciences), CD11b (clone M1/70, BD Biosciences), and hamster anti-mouse CD11c (clone N418, Invitrogen, Eugene, OR) and with LIVE/DEAD Fixable Blue Dead Cell Stain kit (Invitrogen, Eugene, OR). Flow sorting was performed by FACSAria II (BD Biosciences). To remove lymphocytes and neutrophils, live $CD45^+$ singlets were reverse gated on lymphocytes [characteristic forward scatter-area (FSC-A) × side scatter-area (SSC-A)] and neutrophils ($Ly6C^+Ly6G^+$ cells) to select for the following monocyte/macrophage populations: $CD11c^+CD11b^{lo}$ alveolar (Alv) macrophages (Mϕ), $CD11c^+CD11b^+$ activated (Act) Mϕ, $CD11c^{int}CD11b^+$ recruited/transitioning monocyte (Mono)-Mϕ, and $CD11c^-CD11b^+$ Mono. Sal Alv Mϕ and Sal Mono were sorted from the saline treatment group, whereas LPS Act Mϕ, LPS Mono-Mϕ, and LPS Mono were sorted from the LPS-treated group. This gating strategy for these five monocyte/macrophage populations is consistent with previous reports by us and others (40–43).

RNA extraction

Total RNA was extracted from homogenized mouse whole lung cells or from each sorted lung monocyte/macrophage subpopulation single-cell suspension using RNeasy Mini Kit according to the manufacturer's instructions (Qiagen, Germantown, MD). RNA samples were analyzed with respect to purity and potential degradation in the UNMC Genomics Core Facility using a NanoDrop (Thermo Scientific, Nanodrop Products, Wilmington, DE) instrument to measure absorbance. Potential degradation of the sample was assessed by analysis of the RNA using an Advanced Analytical Technical Instrument Fragment Analyzer (AATI, Ames, IA). All samples had A260/280 of 1.8 or above and RQN scores >8.0.

Whole lung RNA-sequencing and analysis

Libraries were generated using 1 µg of total RNA from each sample and the NuGEN Universal Plus mRNA-Seq library kit from TECAN (Redwood City, CA). Libraries were multiplexed and sequenced on the NextSeq550 Sequencer (Illumina) to generate a total of approximately 20 to 25 million 75 bp paired reads for each sample. The original fastq format reads were trimmed by the fqtirm tool (https://ccb.jhu.edu/software/fqtrim) to remove adaptors, terminal unknown bases (Ns), and low-quality 3′ region (Phred score < 30). The trimmed fastq files were processed by FastQC (44) for quality control. The trimmed fastq files were then processed by a standard pipeline utilizing STAR (45) as the aligner and RSEM (46) as the tool for annotation and quantification at the gene level. The raw counts were used for differential expressed gene (DEG) analysis by the R/Bioconductor package DESeq2 (47). The reads were mapped to the mm10 (GRCm38) mouse reference genome. The resulting *p*-values from each comparison were adjusted for false discovery rate (FDR) using the Benjamini–Hochberg (B-H) method (48). The threshold for significant DEGs was B-H-adjusted *p*-value (padj) <0.05. The heatmap was plotted by pheatmap 1.0.12 package in R 4.0.3 based on the value of $\log_2$(TMP_value+0.0001) for all significant genes (adj $p < 0.05$) in all samples to avoid any nonsense values of $\log_2(0)$. The heatmap then underwent symmetric normalization to improve comparative visualization. The volcano plots were created using the GraphPad Prism software, version 10.2.2 (GraphPad, San Diego, CA), with statistical significance accepted at $p < 0.05$. Gene enrichment analyses were performed using Ingenuity Pathway Analysis (IPA; Qiagen Inc., https://www.qiagenbioinformatics.com/products/ingenuity-pathway-analysis). The R package *GOPlot* was utilized to visualize the relationship between genes and enriched pathways. The datasets have been deposited to the Gene Expression Omnibus (GEO) database with access number GSE267022.

NanoString® nCounter expression analysis of monocyte/macrophage subpopulations

For transcriptomic analysis of the three independent experiments of the fluorescence-activated cell sorting (FACS)-isolated five monocyte/macrophage subpopulations from two to four pooled animals per treatment group (saline and LPS) per experiment, the NanoString nCounter system was utilized. The Mouse Myeloid Innate Immunity profiling panel containing 770 genes (NanoString, Seattle, WA) was utilized and run according to the manufacturer's instructions. Sequencing libraries were generated by the UNMC NGS Core beginning with 500 ng of total RNA from each sample using the NuGEN Universal Plus mRNA-Seq library kit from TECAN (Redwood City, CA) following the manufacturer's recommended procedure. Resultant libraries were assessed for size of the insert by analysis of an aliquot of each library on a Bioanalyzer instrument (Agilent Technologies, Santa Clara, CA). Each library had a unique indexing identifier barcode allowing the individual libraries to be multiplexed together for efficient sequencing. Multiplexed libraries were sequenced on a single 150-cycle mid-output flow cell of the NextSeq550 Sequencer (Illumina) using a 2 × 75-bp paired-end protocol to generate a total of approximately 50 million pairs of reads for each sample. The nSolver Analysis Software (NanoString, Seattle, WA) was utilized to compute differential gene expression between two subpopulations. Expression data were normalized to 20 housekeeping genes.

Blood collection and serum

Whole blood was collected from the axillary artery at euthanasia, and serum was harvested as previously described (49). Serum pentraxin-2 (murine acute-phase reactant protein) levels were assessed using a Quantikine ELISA kit (R&D, Minneapolis, MN), according to the manufacturer's instructions [minimal detection difference (MDD) of 0.159 ng/mL].

Lavage fluid cells and lung homogenates

Bronchoalveolar lavage fluid (BALF) was collected from each animal with three 1 mL aliquots of sterile phosphate-buffered saline (PBS, pH 7.4). Total BALF cell counts from pooled lavages were enumerated using a BioRad TC 20 cell counter. Differential cell counts were determined from cytospin-prepared slides (Cytopro Cytocentrifuge, ELITech Group, Logan, UT) with Diff-Quick (Siemens, Newark, DE). Cell-free BALF from the first lavage fraction was evaluated for cytokines and chemokines by murine-specific enzyme-linked immunosorbent assays (ELISA). After BALF isolation and removal of blood from pulmonary vasculature, lung tissue homogenates were prepared by homogenizing lung samples (one-half of each right lung) in 500 µL of sterile PBS. The levels of tumor necrosis factor (TNF)-α, transforming growth factor (TGF)-β, IL-6, IL-10, and the murine neutrophil chemoattractant CXCL1 were quantitated by ELISA (R&D Systems) following the manufacturer's instructions. The kits had MDD of 1.88, 31.3, 1.6, 31.3, and 2.0 pg/mL for TNF-α, TGF-β, IL-6, IL-10, and CXCL1, respectively. Interferon (IFN)-γ was quantitated by ELISA (Invitrogen) with an MDD of 0.7 pg/mL following the manufacturer's instructions. Additionally, lung tissue homogenates were assessed for regulators of extracellular matrix deposition including matrix metalloproteinase (MMP)-3 and tissue inhibitor of metalloproteinase (TIMP)-1 (ELISA; R&D Systems; MDD of 0.125 and 0.031 ng/ml, respectively) as well as MMP-8 and MMP-9 (ELISA; Abcam, Boston, MA; MDD of 0.053 and 0.078 ng/ml, respectively).

Metabolomics: LC-MS/MS analysis of TCA cycle metabolites

To prepare samples, 200 µL of cell-free BALF was added to 1 mL of chilled 80% methanol (LC-MS grade, Thermo Fisher) (13). C_3-pyruvate and $^{13}C_4$-succinate were used as the internal standards and spiked in samples before metabolite extraction. Samples were subsequently centrifuged at 13,000 rpm for 10 min at 4°C. The resulting supernatant was then transferred to a new tube, dried in a SpeedVac (6.5 h, 30°C), and then held at −80°C until metabolomics analysis. Dried samples were reconstituted in 100 µL of 50% methanol. An ultra-performance liquid chromatography *I*-class system (Waters, USA) connected to a triple-quadrupole-ion trap hybrid mass spectrometer (QTRAP6500+, Sciex, USA) was used for the separation and subsequent detection of metabolites of interest. Separation of these metabolites was performed by liquid chromatography using an Acquity UPLC CSH Phenyl-Hexyl column (100 × 2.1 mm ID; 1.7 µm particle size) analytical column procured from Waters, USA, and a binary solvent system with a flow rate of 0.4 mL/min. A CSH Phenyl-Hexyl guard column (20 × 2.1 mm ID; 1.7 µm particle size, Waters) was connected before the analytical column. Mobile phase A was composed of 0.1% formic acid in LC-MS-grade water, whereas mobile phase B was 0.1% formic acid in 100% LC-MS-grade acetonitrile. The column was maintained at 50°C, and the autosampler temperature was maintained at 5°C. The injection volume of each sample was 5 µL, and a total of 500 µL of weak wash solvent comprising 10% aqueous methanol and 500 µL of strong wash solvent comprising 100% acetonitrile were used after each injection. The QTRAP6500 + instrument was operated in polarity switching mode for targeted quantitation of tricarboxylic acid (TCA) cycle metabolites through a multiple reaction monitoring (MRM) process. Electrospray ionization parameters were optimized as follows: electrospray ion voltages of −4,500 and 5,500 V in negative and positive modes, respectively; source temperature of 400°C; curtain gas of 35; and gases 1 and 2 of 40 and 40 psi, respectively. Compound-specific parameters were optimized for each compound using manual tuning. These parameters include the MRMs (Q1/Q3), declustering potentials (DPs), and collision energies (CEs) for each metabolite. These details are listed as follows: lactate (Q1/Q3, DP, CE: 89.0/43.0, −53, −16), citric acid (191.0/111.0, −40, −17.6), pyruvate (87.0/32.0, −46, −14), succinate (117/73, −32, −14), malate (133.0/115.0, −55, −15.6), fumarate (115.0/71.0, −80, −13), α-ketoglutaric acid (145.0/101.0, −40, −13.8), aconitate (173.0/85.0, −40, −17.3), and itaconate (131.0/85.1, 40, 16.8). For each metabolomics run, missing values were estimated by one-third of the minimum positive value of each metabolite. All metabolite values were standardized to CXN mice (n = 5) metabolite average values and therefore represented as fold change relative to CXN.

Lung and lung draining lymph node cell staining and flow cytometry

Lung cell infiltrates were determined following lung cell dissociation from the remaining one-half of each right lung lobe as previously described (49). Pulmonary lymph nodes were harvested from each mouse following published laboratory precedent (50), and a single-cell suspension was achieved by using our previously described protocol for lung dissociation and single-cell suspension (49). For immune cell characterization, cells were stained with fluorophore-conjugated monoclonal antibody against rat anti-mouse CD45 (clone 30-F11, BD Biosciences), CD11b (clone M1/70, BD Biosciences), Ly6G (clone 1A8, BD Biosciences), CD11c (clone N418, Invitrogen), CD4 (clone RM4-5, BD Biosciences), CD8 (clone 53-6.7, BD Biosciences), CD19 (clone 1D3, Invitrogen), CD24 (clone M1/69, BioLegend), hamster anti-mouse CD3e (clone 145-2C11, BD Biosciences), CD103 (clone 2E7, Thermo Fisher), and mouse anti-mouse NK1.1 (clone PK136, BD Biosciences). Cells were then evaluated on a BD LSRII YG (Green Profile) cytometer. In each case, a minimum of 50,000 events were acquired and analyzed for each sample. Post-acquisition, all flow cytometry data were exported and stored

using the flow cytometry standard (FCS) 3.1 format and subsequently analyzed using FlowJo software version 10.10.0 (FlowJo, Ashland, OR). The gating strategies for lung $Ly6G^+$ neutrophils, $CD11c^+CD11b^{lo}$ Alv Mϕ, $CD11c^+CD11b^+$ Act Mϕ, $CD11c^{int}CD11b^+$ Mono-Mϕ, and $CD11c^-CD11b^+$ Mono, $CD3^+CD4^+$ T cells, $CD3^+CD8^+$ T cells, $CD19^+$ B cells, and NK cells were performed as previously reported (Supplementary Figure 1) (15, 39, 51–54). In a separate experiment, whole lungs of LPS-exposed WT (n = 5) and *Acod1*$^{-/-}$ (n = 5) mice were harvested 48 h post-LPS exposure, homogenized, and stained to characterize dendritic cells via flow cytometry. Briefly, after the removal of debris, doublets, dead cells, $CD45^-$ cells, lymphocytes, neutrophils, and $CD11b^+$ cells, $CD11c^+$ cells were quadrant gated by CD24 and CD103 expression to delineate $CD103^+$ and $CD103^-CD24^+$ dendritic cells (55). The gating strategies for lymph node $Ly6G^+$ neutrophils, $Ly6C^{hi}CD11b^{hi}$ monocytes, $CD11c^{hi}CD11b^{variable}$ macrophages, $CD3^+CD4^+$ T cells, $CD3^+CD8^+$ T cells, $CD19^+$ B cells, NK cells, and dendritic cells were informed by previously reported work (Supplementary Figure 2) (55–57). The percentage of all respective lung cell populations was determined from live $CD45^+$ lung leukocytes after excluding debris and doublets. This percentage was multiplied by the respective total lung cell numbers to determine specific cell population numbers for each animal. Lymph node-specific cell populations are represented by the percent of $CD45^+$ cells where immune cell numbers are standardized to the $CD45^+$ cell number per biologic sample and multiplied by 100.

Lung myeloid cell functional assays

In separate studies, phagocytic ability and reactive oxygen species (ROS) production were determined for lung monocytes/macrophages and neutrophils from whole lung cells of the *in-vivo* LPS-exposed WT and *Acod1*$^{-/-}$ mice. At 48 h post-exposure, single lung cell suspensions were incubated for 30 min at 37°C with 25 µM of CellROX Deep Red (Invitrogen, Carlsbad, CA) or with opsonized, fluorescein-conjugated *E. coli* BioParticles (Invitrogen, Carlsbad, CA) to quantify ROS and phagocytic activity according to the manufacturers' instructions, respectively. Cells were then placed on ice and incubated as described above for markers indicative of monocytes, macrophages, and neutrophils (i.e., live/dead, CD45, CD11b, CD11c, Ly6G). Cells were subsequently washed with cold PBS, fixed with 4% paraformaldehyde, and analyzed on a BD LSRII YG (Green Profile). The gating strategy for the neutrophils and monocyte/macrophage subpopulations is consistent with that shown in Supplementary Figure 1. Lung $Ly6G^+$ neutrophils, $CD11c^+CD11b^{lo}$ alveolar macrophages, $CD11c^+CD11b^+$ activated macrophages, $CD11c^{int}CD11b^+$ monocytes–macrophages, and $CD11c^-CD11b^+$ monocytes were analyzed for CellROX- and BioParticles-associated fluorescence as previously described (18). Data are represented by the percent of the cell population that exhibited BioParticles- (%BioParticles+) or CellROX-specific (%CellROX+) probe fluorescence. Additionally, mean fluorescence intensity (MFI) was quantified and compared per cell population between WT and *Acod1*$^{-/-}$ mice.

Lung histopathology and Masson's modified trichrome staining

Left lungs were excised and inflated to 15 cm H_2O pressure with 10% formalin (Fisher Scientific, Fair Lawn, NJ) for 24 h to preserve pulmonary architecture as previously described (49). The fixed lobes were then placed into cassettes, embedded in paraffin, cut (to 4–5 µm) at midpoint sections to include regions of both large and small airways as well as blood vessels, and stained with hematoxylin and eosin (H&E). Slides were then reviewed at all scanning magnifications by an experimental pathologist blinded to the treatment conditions and semiquantitatively assessed for the degree and distribution of lung inflammation. Using a previously published scoring system, each lung was given an inflammatory score value from 1 to 4 (a higher score indicating greater inflammatory changes in the lung) (58). Lung sections were also stained with modified Masson's trichrome and scanned with an Aperio scanner (Leica Biosystems, Deer Park, IL) by the institution's Tissue Sciences Core Facility. Aperio ImageScope Software (Leica Biosystems, Deer Park, IL) was utilized to export lung sections at full resolution in TIFF format. Collagen staining of the whole lung images was isolated with ImageJ FIJI software (version: 2.9.0/1.53t U.S. National Institutes of Health, Bethesda, MD) and the Colour Deconvolution plugin (59) using methods to create a user-defined color matrix as described by the plugin authors. The integrated density of the isolated collagen staining was then measured using a static thresholding scheme as previously described (15).

Invasive pulmonary function measurement

Altered lung function is a hallmark characteristic of lung inflammation (60). Although AHR is a canonical feature of allergic asthma, AHR can also be induced by ozone exposure, viral infection, lipopolysaccharide, and agricultural exposure (61–64). Baseline airway resistance and compliance as well as AHR was invasively assessed by direct airway resistance, 3 h post-i.t.-instilled LPS or saline, using a computerized small-animal ventilator (FinePointe, Buxco Electronics, Wilmington, NC), as previously described (65). Dose responsiveness to aerosolized methacholine (0–48 mg/mL) was obtained and is reported as total lung resistance (R_L). Our previous work and others have demonstrated peak AHR at 3–5 h post-LPS enriched exposures with loss of AHR 24 h post-exposure (63, 65, 66), informing the 3-h timepoint for AHR testing.

Statistical analysis

Sample-size requirements were extrapolated from a previous work assessing post-LPS lung recovery treatments in C57BL/6 (15). The mean (± SD) of $CD11c^{int}CD11b^{hi}$ transitioning/recruited Mono-MΦ was 0.26×10^5 (0.09×10^5) with saline and 6.5×10^5 (2.2×10^5) with LPS treatment 48 h post-exposure; thus, a sample size of n = 2 in each group would achieve 80% power at the 0.05 level of significance to determine an influx of these cells following

inflammatory agent exposure as compared to saline control. Littermates and purchased mice were used to achieve the following sample size per treatment group: n = 5 (5 male WT, Saline; referred to as CXN), n = 19 (9 male and 10 female WT, LPS), n = 18 (8 male and 10 female *Acod1*$^{-/-}$, LPS), n = 17 (7 male and 10 female WT, ODE), and n = 19 (9 male and 10 female *Acod1*$^{-/-}$, ODE). Numbers less than the maximum number reflect limitations in the available sample quantity or quality. Data are presented as the mean ± standard error of the mean (± SEM) with scatter plots depicted for each data point. The Shapiro–Wilk test was utilized to test for normality among treatment groups. If the normality condition was satisfied, a parametric statistical test (one-way ANOVA with subsequent Tukey's multiple comparison test) was used, and if not satisfied, a non-parametric statistical test (Kruskal–Wallis with subsequent Dunn's multiple comparison test) was used to assess differences between any two groups. All statistical analyses were performed using GraphPad Prism (version: 10.2.2) software, and statistical significance was accepted at a p-value <0.05 unless otherwise specified.

Ethics statement

Neither human participants, data, nor tissues were used in these experiments. The study was conducted and reported in accordance with ARRIVE guidelines (https://arriveguidelines.org). All animal procedures were approved by the University of Nebraska Medical Center (UNMC) Institutional Animal Care and Use Committee and were in accordance with NIH guidelines for the use of rodents.

Results

Bioinformatical analysis of the whole lung transcriptome following lung-delivered LPS

To identify unique regulatory transcripts and potential therapeutic targets following inhalant LPS exposure, bulk RNA sequencing (RNA-seq) of whole lung tissue processed from saline-treated (n = 3) and 10 μg of LPS-treated (n = 3) animals was examined 48 h after challenge. Of the 20,749 genes identified, 6,515 demonstrated significant changes (p < 0.05) in expression between treatment groups. There were 3,163 genes that were significantly upregulated, whereas 3,352 genes were significantly downregulated. Differential expression analysis (DEA) was performed by comparing the whole lung transcriptome between LPS- and saline-exposed mice with unsupervised hierarchical clustering delineating these distinct transcriptomes (Figure 1A). A volcano plot shows differential gene expression achieving statistical significance (p < 0.05) with its magnitude of fold change ($\log_2$FoldChange > 1) in LPS-exposed relative to saline-exposed mice. The top canonical pathways (padj < 0.05) and their top enriched genes (p < 0.05) in mice exposed to LPS are demonstrated in the chord plot (Figure 1C). *Acod1* was significantly upregulated (28th most upregulated transcript of 3,163 significantly upregulated genes) in these comparative transcriptomic investigations (Figure 1B) and defined as a driver of the macrophage classical activation signaling pathway (Figure 1C). IPA of the whole lung transcriptome implicated pathways canonically associated with inflammatory cell recruitment, immune cell signaling, wound healing, and classical macrophage activation following lung exposure to LPS (Figure 1C).

LPS exposure induces transcriptional reprogramming in the lung monocyte/macrophage compartment

To characterize transcriptomic changes specific to lung monocyte/macrophage subpopulations post-LPS exposure, we defined the differential gene expression of distinct populations of infiltrating lung cells. Lung monocyte/macrophage subpopulations were FACS-isolated based on relative CD11b and CD11c surface expression of live, singlet, CD45$^+$ cells that were neither neutrophils nor lymphocytes (Figure 2A). Consistent with previous studies (15), at 48 h post-LPS exposure, "resting" alveolar macrophages (referred to as Sal Alv MΦ) are "lost" as they upregulate CD11b and now exhibit an activated phenotype (referred to as LPS Act MΦ). The LPS-activated monocyte/macrophage subpopulations (LPS Act MΦ, LPS Mono-MΦ, and LPS Mono) demonstrated distinctive transcriptomic profiles relative to saline-exposed subpopulations (Sal Alv MΦ and Sal Mono) with universal upregulation of regulatory transcripts across LPS-exposed subpopulations (Figure 2B). There were inadequate numbers of Sal Mono-MΦ for experimental studies. To further elucidate the characteristics of the LPS-induced Mono-MΦ subpopulation, its transcriptomic profile was compared to both Sal Alv MΦ and Sal Mono (Figure 2B). *Acod1* was universally upregulated ($\log_2$FoldChange) in the LPS Act MΦ vs. Sal Alv MΦ (3.2), LPS-Mono-MΦ vs. Sal Alv MΦ (7.49), and LPS Mono vs. Sal Mono (4.07) subpopulations but did not reach statistical significance (p > 0.05) with the LPS Act MΦ vs. Sal Alv MΦ comparison. The LPS Act MΦ vs. Sal Alv MΦ comparison yielded the most distinctive upregulated gene profile, given there was no overlap between these top 10 most upregulated genes and the top 10 most upregulated genes across the remaining three comparisons.

The top 5 most significantly (p < 0.05) upregulated genes for the LPS Act MΦ vs. Sal Alv MΦ comparison included *Ear6* (2.32), *Yap1* (1.33), *Fgf2* (1.12), *Abcc8* (0.91), and *Cd70* (0.76). There were three gene transcripts that were among the top 10 most upregulated across all remaining comparisons (LPS Mono vs. Sal Mono, LPS Mono-MΦ vs. Sal Alv MΦ, and LPS Mono-MΦ vs. Sal Mono): *Nos2* (5.36, 9.05, and 7.35, respectively), *Il12a* (4.35, 7.24, and 5.8), and *Ccl5* (3.68, 7.36, and 6.27). In comparison to LPS Mono vs. Sal Mono and LPS Mono-MΦ vs. Sal Alv MΦ, both *CD38* ($\log_2$FoldChange: 4.56 and 7.09, respectively) and *Ccl12* (3.71 and 7.6) were among the top 10 most significantly upregulated transcripts. In the LPS Mono vs. Sal Mono and LPS Mono-MΦ vs. Sal Mono comparisons, *Cxcl9* (6.21 and 6.87), *Il12b* (4.02 and 6.99), and *Cxcl3* (3.65 and 7.59) were among the top 10 most significantly upregulated gene transcripts, respectively. Gene transcripts that were unique to a comparison's top 10 most significantly upregulated genes are as follows: LPS Mono vs. Sal

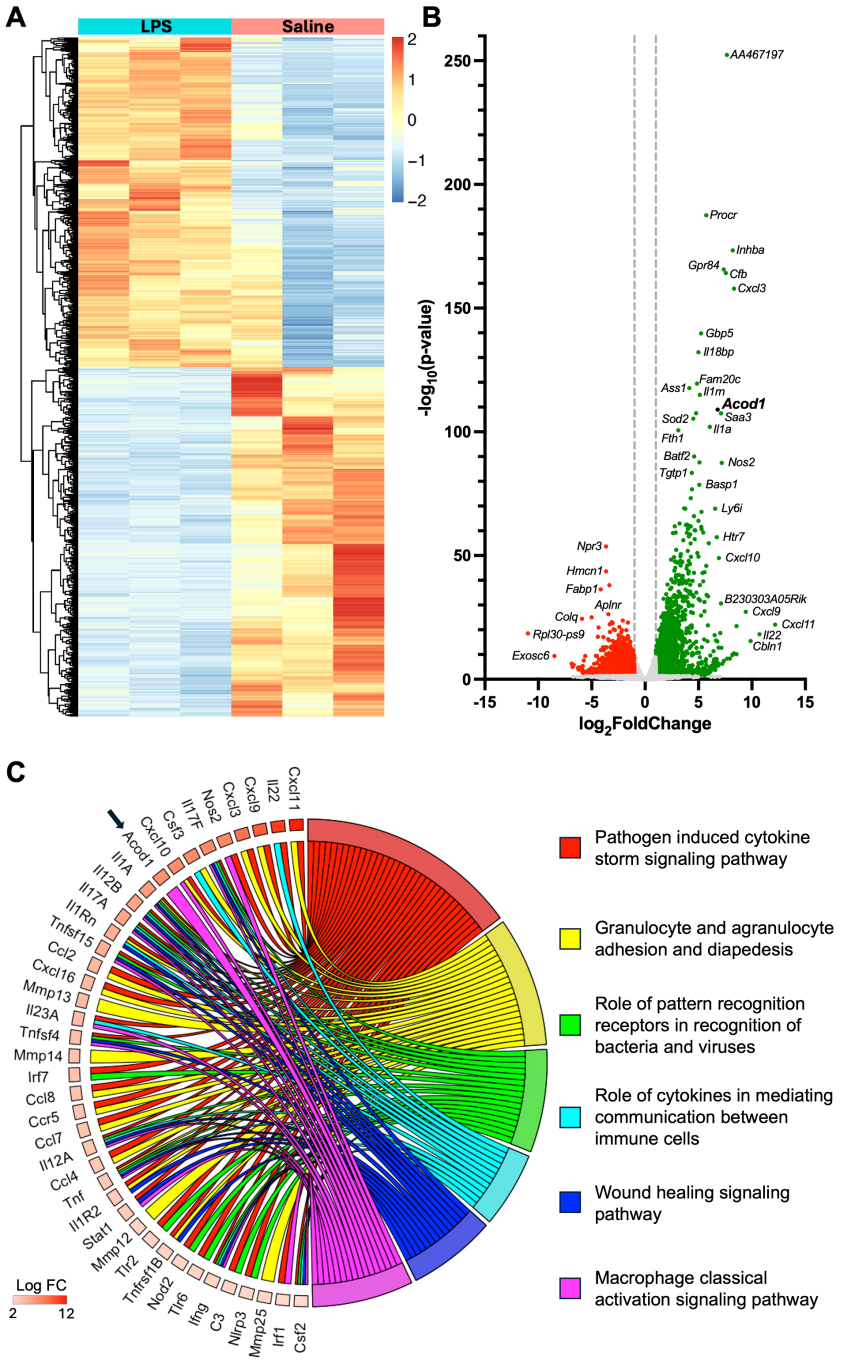

FIGURE 1
Comparative transcriptome of lung tissue from lipopolysaccharide (LPS)- and saline-exposed mice at 48 h post-exposure. **(A)** Heatmap demonstrates unsupervised hierarchical clustering of samples (n = 3 per treatment) and relative frequencies of genes subjected to symmetric normalization of $\log_2$(transcripts per million [TPM] + 0.0001) for all significant genes (adj $p < 0.05$) to avoid any nonsense values. The color scheme represents symmetric normalization of relative frequencies from 2 (red, high expression) to −2 (blue, low expression). **(B)** Volcano plot demonstrates statistical significance ($-\log_{10}$(p-value)) vs. magnitude of change ($\log_2$FoldChange) in the expression of specified gene transcripts ($-\log_{10}$(p-value) > 1.3) with green reflecting upregulated and red reflecting downregulated genes. **(C)** Chord plot demonstrates the top canonical pathways of the whole lung transcriptome based on the Ingenuity Pathway Analysis (IPA) output and corresponding adjusted p-value (adj $p < 0.05$) and the top upregulated genes ($p < 0.05$) associated with each modulated pathway.

Mono: *Cxcl11* (4.7) and *Il1rn* (3.81); LPS Mono-MΦ vs. Sal Alv MΦ: *Ly6c1* (7.93), *Cxcl9* (7.72), *Acod1* (7.49), *Cxcl10* (7.48), and *Aoah* (7.31); LPS Mono-MΦ vs. Sal Mono: *Arg1* (5.89), *Il1a* (5.75), *Cxcl16* (5.7), and *Ccl22* (5.67). The distinctive transcriptomes among the monocyte/macrophage subpopulations emphasize the heterogeneity of the lung monocyte/macrophage compartment and identify potential regulatory targets that merit further investigation. *Acod1* is of particular interest given that it is highly upregulated at both the whole lung and monocyte/macrophage resolution. Given the cellular specificity of ACOD1 to monocytes/macrophages,

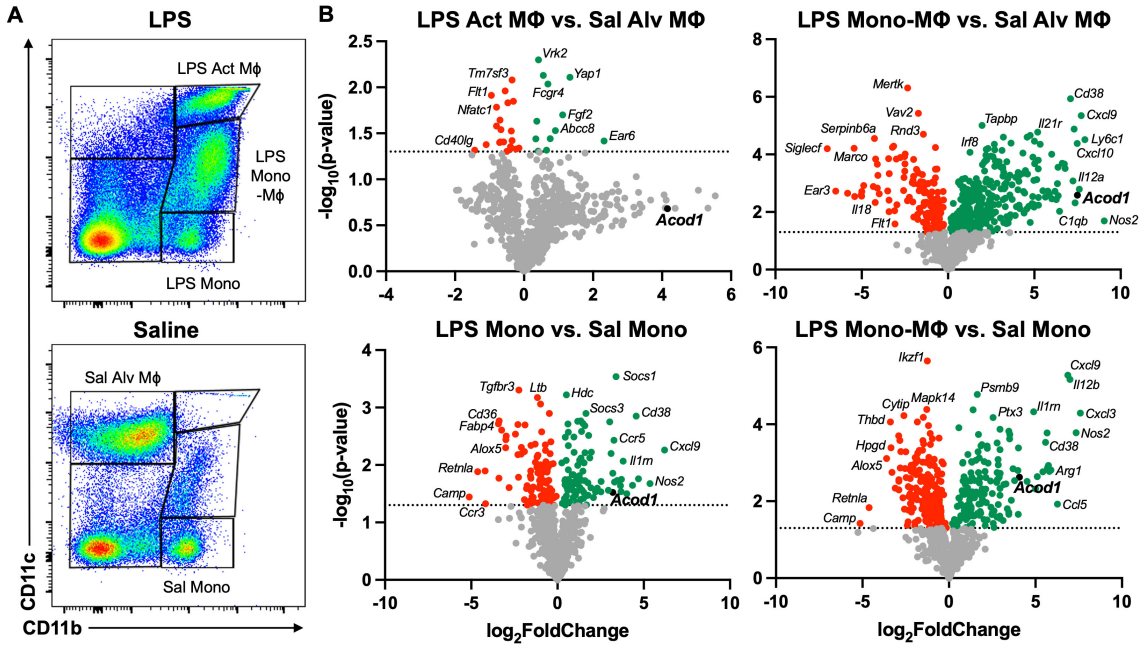

FIGURE 2
Acute exposure to LPS differentially modulates myeloid cell gene transcription with notable *Acod1* upregulation. **(A)** Representative image of gates for the five lung monocyte (Mono)/macrophage (MΦ) subpopulations: Saline (Sal) Alveolar (Alv) MΦ: $CD11c^{+}CD11b^{lo}$, LPS Activated (Act) MΦ: $CD11c^{+}CD11b^{hi}$, Transitioning LPS Mono-MΦ: $CD11c^{int}CD11b^{hi}$, and Sal and LPS Mono: $CD11b^{hi}CD11c^{-}$ after exclusion of debris, doublets, dead cells, $CD45^{-}$ cells, lymphocytes, and neutrophils. **(B)** Volcano plots demonstrate statistical significance ($-\log_{10}$(*p*-value) vs. magnitude of change ($\log_2$FoldChange) in the expression of specified gene transcripts. Statistical significance is denoted by the dotted line ($-\log_{10}$(*p*-value) > 1.3). *n* = 3 samples per lung monocyte/macrophage subpopulation for differential gene expression analysis.

modulation of this regulatory molecule will mitigate off-target effects and alter the functionality of these cellular populations, which are integral to disease pathogenesis (67). As such, the following studies focused on characterizing the role of ACOD1 in environmental exposure-induced lung inflammation.

Acod1 depletion reduces LPS- and ODE-induced serum pentraxin-2 levels but not LPS- or ODE-induced weight loss

To characterize the functional role of ACOD1 in mediating the inflammatory response to a one-time, lung-targeted inflammatory agent (LPS and ODE), C57BL/6NJ (WT) and C57BL/6NJ-*Acod1*$^{em1(IMPC)J}$/J (*Acod1*$^{-/-}$) mice were i.t. instilled with either LPS (10 µg), 25% ODE, or saline (Control; CXN) with endpoints collected 48 h post-exposure (schematic, Figure 3A). Weights were collected to assess the systemic response to inhaled environmental exposures, and serum pentraxin-2, a murine acute-phase reactant protein, was quantified to assess systemic responsiveness to inflammatory stimuli. Mouse serum pentraxin-2 is produced by hepatocytes and induced by IL-6 (similar to human C-reactive protein), making it an appropriate biomarker representative of non-specific, systemic inflammation (68). LPS- and ODE-induced weight loss was not dependent on *Acod1* (Figure 3B). However, LPS- and ODE-induced serum pentraxin-2 was decreased in the *Acod1*$^{-/-}$ mice, reaching significance ($p < 0.05$) for ODE-WT vs. *Acod1*$^{-/-}$ mice but not LPS-WT vs. *Acod1*$^{-/-}$ animals (Figure 3C).

ACOD1 alters carbohydrate metabolism in the airway through TCA cycle modulation

The purpose of this targeted metabolomic investigation by mass spectrometry was two-fold: 1) validate effective *Acod1* deletion in the *Acod1*$^{-/-}$ mice by itaconate quantification and 2) characterize the downstream metabolic effects of ACOD1 removal on the TCA cycle in our model system. Relative BALF metabolite quantities are presented as fold change of LPS or ODE exposure relative to CXN (saline-treated). Itaconate levels were significantly decreased in *Acod1*$^{-/-}$ as compared to WT or *Acod1*-sufficient mice (Figure 4). Thus, *Acod1*$^{-/-}$ mice have sufficient ACOD1 deletion to yield observable differences in BALF itaconate concentrations following environmental inflammatory agent exposure. Metabolic disturbances downstream of ACOD1 were only identified in the LPS-exposed mice where *cis*-aconitate, α-ketoglutaric acid, fumarate, and malate were significantly increased in *Acod1*$^{-/-}$ mice as compared to WT (Figure 4).

Cellular infiltrates and inflammatory mediators are dependent on ACOD1 following LPS exposure in the lung

To characterize the role of ACOD1 in mediating local, inflammatory processes, lung tissue and BALF from WT and *Acod1*$^{-/-}$ animals were harvested 48 h post-i.t. LPS and assessed for cellular composition and inflammatory indicators. In the LPS-

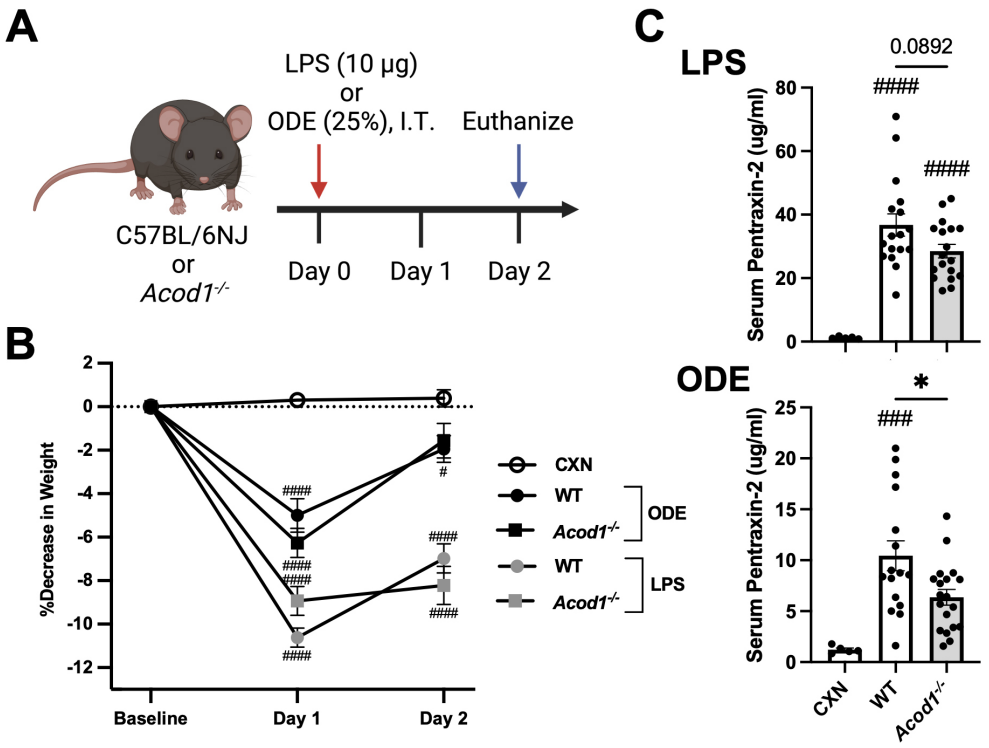

FIGURE 3
Acod1 depletion decreases ODE-induced serum pentraxin-2 levels but not LPS- or ODE-induced weight loss. **(A)** Schematic of the experimental design (created with BioRender.com). **(B)** Line graph depicts the mean with SEM bars of percent changes in weight over time. **(C)** Scatter plot graphs depict the mean with SEM bars of serum pentraxin-2 levels among treatment groups. n = 5 (CXN), n = 17–19 (8–9 male and 9–10 female WT mice, LPS), n = 18 (8 male and 10 female *Acod1*$^{-/-}$ mice, LPS), n = 16–17 (7 male and 9–10 female WT mice, ODE), and n = 19 (9 male and 10 female *Acod1*$^{-/-}$ mice, ODE). Statistical significance vs. CXN (#p < 0.05, ###p < 0.001, ####p < 0.0001); between groups (*p < 0.05).

exposed mice, BALF neutrophil influx was decreased in *Acod1*$^{-/-}$ mice relative to WT, despite no significant differences in total cells (Figure 5A). LPS-induced lung CD4$^+$ T-cell infiltrates were decreased in *Acod1*$^{-/-}$ vs. WT animals, and there were no differences between WT and *Acod1*$^{-/-}$ mice regarding LPS-induced neutrophils, monocytes, and B-cell infiltrates (Figure 5B). LPS-induced BALF levels of TNF-α and CXCL1, but not IL-6, were decreased in *Acod1*$^{-/-}$ mice vs. WT mice (Figure 5C). Lung levels of TNF-α (but not IL-6 and CXCL1) induced by LPS were also reduced in *Acod1*$^{-/-}$ vs. WT mice (Figure 5C). Additional efforts to characterize the difference in LPS-induced airway inflammatory responses between WT and *Acod1*$^{-/-}$ mice that did not achieve statistical significance are included in Supplementary Table 1. There were no significant differences between LPS-treated WT (n = 5) and *Acod1*$^{-/-}$ (n = 5) mice regarding lung dendritic cell populations. Neither the number of CD103$^+$CD24$^+$ dendritic cells (WT mean ± SEM vs. *Acod1*$^{-/-}$ mean ± SEM: 0.609 ± 0.294 × 10^5 vs. 0.344 ± 0.035 × 10^5; p = 0.397) nor the number of CD103$^-$CD24$^+$ dendritic cells (2.98 ± 1.01 × 10^5 vs. 1.37 ± 0.097 × 10^5; p = 0.152) in whole lung samples was altered between WT and *Acod1*$^{-/-}$ mice. No significant differences in cellular composition were observed between WT and *Acod1*$^{-/-}$ pulmonary draining lymph nodes following a one-time LPS exposure (Supplementary Table 3). ACOD1 appears to participate in the lung proinflammatory response to LPS given the elevated inflammatory markers and cellular infiltrates in *Acod1*$^{-/-}$ vs. WT mice.

ODE exposure-induced cellular influx and proinflammatory mediators are reduced in *Acod1*$^{-/-}$ mice

In separate studies, the effects of ODE exposure in WT and *Acod1*$^{-/-}$ mice were also evaluated to characterize the role of ACOD1 in coordinating inflammation in response to a more complex, environmentally relevant exposure. ODE-induced total cellular influx in the BALF compartment was decreased in *Acod1*$^{-/-}$ mice relative to WT without a significant change in neutrophils (Figure 6A). ODE-induced lung neutrophil, monocyte, and B-cell infiltrates, but not CD4$^+$ T cells, were decreased in *Acod1*$^{-/-}$ vs. WT mice (Figure 6B). BALF levels of ODE-induced TNF-α and IL-6 and lung levels of CXCL1 were also decreased in *Acod1*$^{-/-}$ mice relative to WT (Figure 6C). Supplementary Table 2 includes additional data characterizing ODE-induced airway inflammatory consequences between *Acod1*$^{-/-}$ and WT mice that did not statistically differ. ACOD1 therefore seems necessary to coordinate the characteristic, proinflammatory lung response to ODE exposure given the elevated proinflammatory phenotype observed in *Acod1*$^{-/-}$ vs. WT mice.

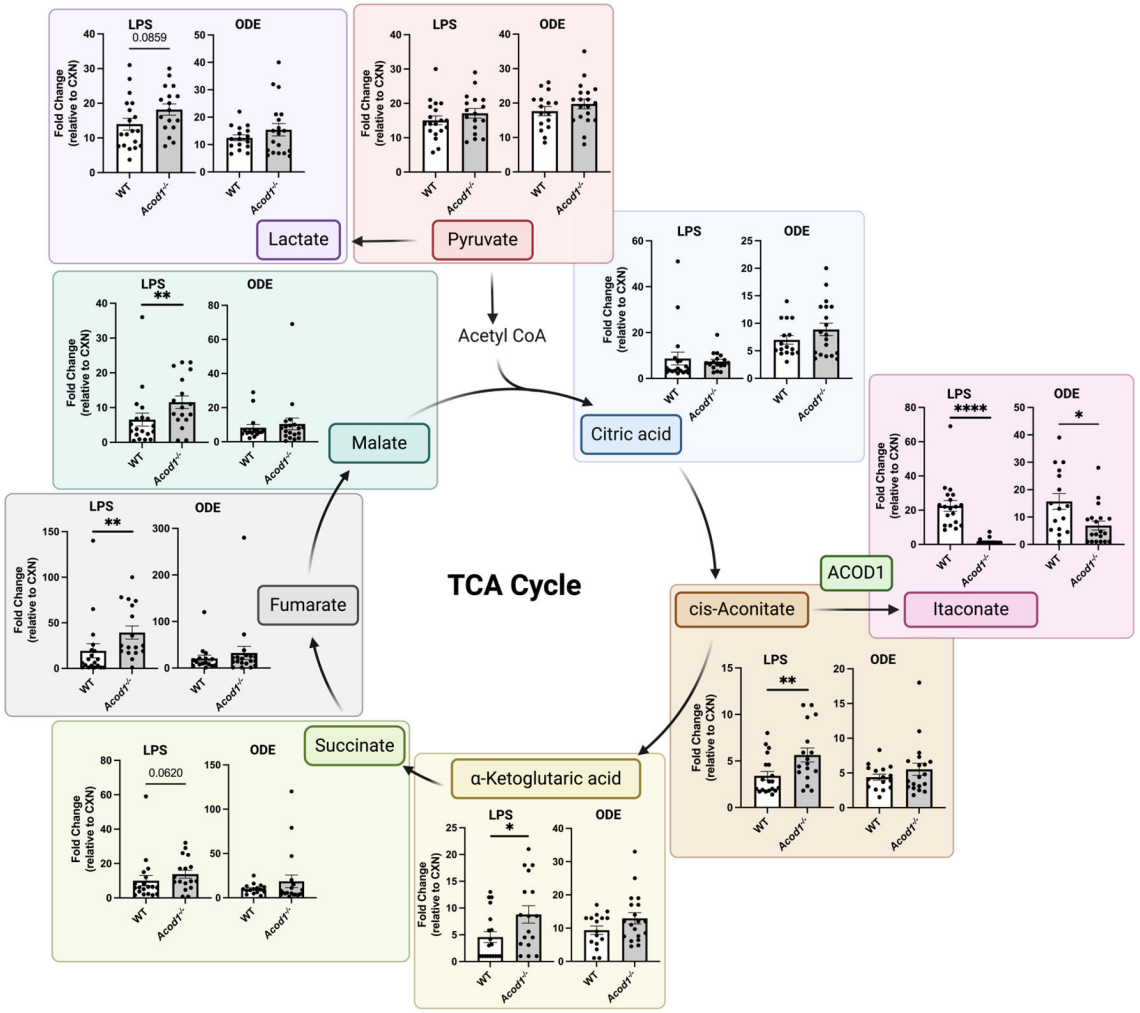

FIGURE 4
Acod1$^{-/-}$ mice demonstrate modulation of tricarboxylic acid cycle (TCA) intermediates following environmental exposure. A simplified schematic of the TCA cycle with scatter plot graphs depicting the mean with SEM bars between treatment groups. Graphs show the relative abundance of indicated metabolites, represented by fold change relative to CXN (saline-treated WT mice). n = 5 (CXN), n = 19 (9 male and 10 female WT mice, LPS), n = 18 (8 male and 10 female *Acod1*$^{-/-}$ mice, LPS), n = 17 (7 male and 10 female WT mice, ODE), and n = 19 (9 male and 10 female *Acod1*$^{-/-}$ mice, ODE). Statistical significance between groups (*p < 0.05, **p < 0.01, ****p < 0.0001).

ACOD1 does not significantly alter functional characteristics of myeloid-derived subpopulations post-LPS exposure

To determine whether ACOD1 deficiency impacted the functional consequences of lung myeloid cells in the setting of *in-vivo* LPS exposure, assays capturing phagocytic activity and intracellular ROS were undertaken. The only significant difference was between WT and *Acod1*$^{-/-}$-activated macrophages (Act Mϕ; CD11c^{+}CD11b^{+}) whereby *Acod1*$^{-/-}$ Act Mϕ exhibited elevated intracellular ROS as quantified by MFI of the CellROX+ population (Table 1). Otherwise, there were no differences in ROS production or phagocytic ability as measured by the ability to uptake bioparticles between LPS-exposed WT and *Acod1*$^{-/-}$ monocyte/macrophage subpopulations or neutrophils. Thus, despite decreased indicators of inflammation/injury in *Acod1*$^{-/-}$ mice, indices of lung myeloid cell function appear preserved across cellular populations, indicating that phagocytic ability and ROS production induced by LPS exposure are not attributable to ACOD1.

LPS-induced mediators of tissue remodeling and AHR were dependent on ACOD1

Other studies have demonstrated significant increases in lung MMPs during the acute phase of lung injury in animal models of lung injury resulting from LPS (by 48 h), hypoxia (peak at 72 h), hyperoxia (at 48 h), and bleomycin (by day 4) (19, 69). Given monocyte/macrophage subpopulations coordinate the transitions from acute inflammation to lung repair to aberrant fibrosis (11), we sought to determine whether ACOD1 influenced profibrotic processes and lung function at this early timepoint. LPS-induced

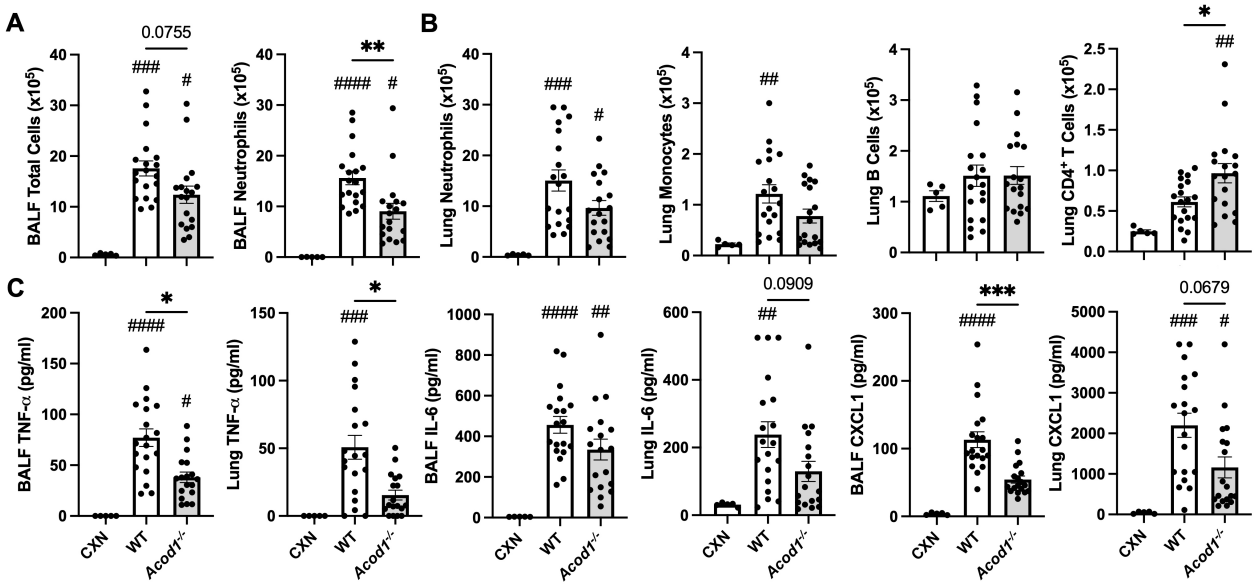

FIGURE 5
LPS-induced cellular infiltrates and inflammatory mediators are reduced in *Acod1*$^{-/-}$ mice. Scatter plot graphs depict the mean with SEM bars among treatment groups. **(A)** Total cellular influx and neutrophils in BALF. **(B)** Neutrophils, monocytes, B cells, and CD4^{+} T cells in lung tissue quantified by flow cytometry. **(C)** Levels of airway inflammatory markers determined by ELISA from BALF and lung homogenate. n = 5 (CXN), n = 19 (9 male and 10 female WT mice), and n = 18 (8 male and 10 female *Acod1*$^{-/-}$ mice). Statistical significance vs. CXN (#p < 0.05, ##p < 0.01, ###p < 0.001, ####p < 0.0001); between groups (*p < 0.05, **p < 0.01, ***p < 0.001).

lung levels of profibrotic mediators including TIMP-1, MMP-8, and MMP-9 were reduced in *Acod1*$^{-/-}$ vs. WT mice (Figure 7). Although these findings were not mirrored in ODE-exposed animals, MMP-9 was significantly reduced in *Acod1*$^{-/-}$ vs. WT mice (Figure 7). LPS- and ODE-induced MMP-3 did not significantly differ between *Acod1*$^{-/-}$ and WT mice (Supplementary Tables 1, 2). Relative to control (CXN) treatment, LPS exposure increased the levels of TGF-β and IFN-γ, whereas ODE only increased the levels of TGF-β in WT and *ACOD1*$^{-/-}$ mice; however, there were no significant differences between LPS- or ODE-treated WT and *ACOD1*$^{-/-}$ mice (Supplementary Tables 1, 2). No changes between WT and *Acod1*$^{-/-}$ mice were observed regarding histologic scoring of lung tissue sections or collagen quantification via Masson's trichrome staining (Supplementary Figure 3). Acute environmental exposure-induced airway hyperresponsiveness is a phenomenon that has been observed in humans and modeled in mice (70). No differences in AHR were observed between WT and *Acod1*$^{-/-}$ mice exposed to saline (Figure 8). Interestingly, *Acod1*$^{-/-}$ mice displayed a significant reduction in LPS-induced AHR, compared to WT mice, at methacholine doses greater than 12 mg/mL (Figure 8). ACOD1 observably elevated the profibrotic and adverse functional consequences associated with an inhaled, LPS exposure.

Discussion

LPS-enriched organic dusts are critical drivers of environmental lung inflammation and disease (71, 72). Here, our investigations first characterized the mouse lung transcriptome as well as transcriptomic changes across monocyte/macrophage subpopulations following a lung-delivered LPS exposure. Both studies demonstrated striking differences, with pathway enrichment analysis of LPS-induced whole lung transcriptomic changes implicating inflammatory cell recruitment, classical macrophage activation, cytokine-mediated signaling, pattern recognition receptor activation, and tissue repair pathways. ACOD1 expression was strikingly upregulated following LPS exposure in the whole lungs and in the following monocyte/macrophage subpopulations: LPS Act Mϕ, LPS Mono-Mϕ, and LPS Mono. Furthermore, investigations into the functional significance of ACOD1 following LPS and ODE exposures demonstrated that ACOD1 mediates proinflammatory responses and airway hyperresponsiveness to environmentally relevant exposures.

The heterogeneity of the monocyte/macrophage lung compartment is increasingly appreciated in several lung diseases, including those associated with environmental and occupational exposures. Specifically, the recruited, transitioning monocytes–macrophages have been implicated as critical cells in the immunopathogenesis of chronic lung disease with an environmental etiology (15, 73). Whereas it has also been demonstrated that depleting the recruitable reservoir of circulating monocytes results in favorable lung inflammatory consequences following LPS exposure in mice, the translational application of this approach is not infeasible. Other strategies aimed at mitigating monocyte/macrophage recruitment via targeting the CCR2 (a marker of inflammatory monocytes) failed to reduce LPS-induced airway disease in mice (19, 74). Thus, other strategies to reduce the recruitment and/or activation status of this transitioning monocyte–macrophage subpopulation are warranted.

Our monocyte/macrophage subpopulation-specific transcriptomic characterization could elucidate new targets to more specifically and

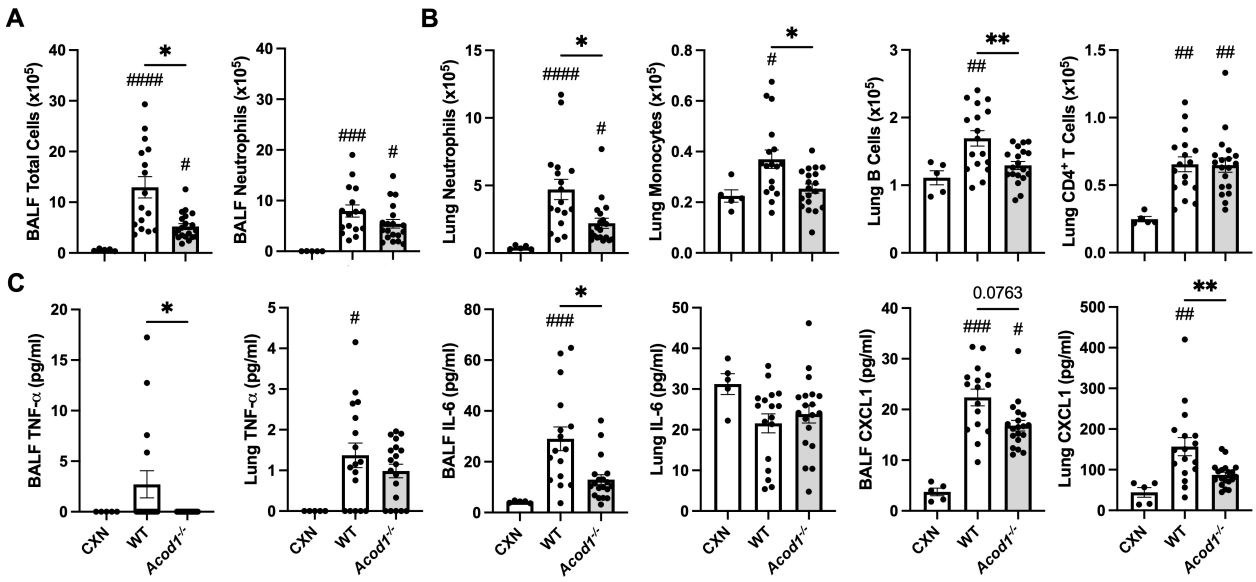

FIGURE 6
Acod1$^{-/-}$ mice exhibit decreased mediators of lung and airway inflammation following a one-time ODE exposure. Scatter plot graphs depict the mean with SEM bars among treatment groups. **(A)** Total cellular influx and neutrophils in BALF. **(B)** Neutrophils, monocytes, B cells, and CD4^{+} T cells in lung tissue quantified by flow cytometry. **(C)** Levels of airway inflammatory markers determined by ELISA from BALF and lung homogenate. n = 5 (CXN), n = 16–17 (7 male and 9–10 female WT mice exposed to ODE), and n = 19 (9 male and 10 female *Acod1*$^{-/-}$ mice exposed to ODE). Statistical significance vs. CXN (#p < 0.05, ##p < 0.01, ###p < 0.001, ####p < 0.0001); between groups (*p < 0.05, **p < 0.01).

robustly reduce the recruitment and/or activation of these infiltrating cells. *Ccl5* was upregulated on all LPS-activated monocyte/macrophage subpopulations and is a chemokine that primarily recruits T cells, monocytes, and dendritic cells (75). Targeted inhibition of CCR1, CCR5, or CCL5 could decrease monocyte recruitment as CCL5 mediates cellular recruitment to areas of inflammation (76, 77). Reactive nitrogen and oxygen species have been heavily implicated in environmental exposure-induced lung inflammation (78). Predictably, *Nos2* was significantly upregulated among all LPS-exposed subpopulations. NOS2 inhibitors may mitigate inflammatory consequences and associated tissue damage as a standalone or adjunctive therapy (79). *Ly6c1* was among the most upregulated transcripts in the Mono-MΦ subpopulation, and Ly6C^{hi} macrophages derived from circulating Ly6C^{hi} monocytes have been well-characterized as having proinflammatory and profibrotic functions (80). Therefore, targeting this specific population of Ly6C^{hi}CD11c^{int}CD11b^{+} Mono-MΦ may elicit therapeutic benefit by modulating the acute inflammatory response and mitigating associated fibrotic processes. Finally, *Acod1* was a distinguishing transcript of the LPS Mono-MΦ, especially relative to Alv MΦ, and moreover, it was the 28th most upregulated transcript in the LPS-exposed lung transcriptome. These observations informed our subsequent efforts to characterize the role of ACOD1 in mediating exposure-induced lung inflammation.

We discovered that ACOD1 is capable of mediating differential metabolic consequences depending on the complexity and composition of the environmental exposure (i.e., LPS or ODE exposure). Both the LPS and ODE exposures demonstrated decreased levels of itaconate in the absence of ACOD1; however, only the LPS-exposed mice exhibited altered carbohydrate metabolism downstream of ACOD1 where relative abundances of *cis*-aconitate, α-ketoglutaric acid, fumarate, and malate were increased in *Acod1*$^{-/-}$ mice relative to WT. Elimination of the ACOD1-mediated carbohydrate shunt in *Acod1*$^{-/-}$ mice likely resulted in corresponding increases in downstream metabolites only in LPS-exposed mice. There are potential explanations that could account for the difference in LPS- and ODE-induced metabolomic effects. First, LPS was a stronger inducer of tightly linked macrophage activity and metabolism. Next, non-LPS components of the highly complex ODE may be modulating immunometabolic perturbations. Namely, previous findings have demonstrated that the endotoxin component in swine barn dust does not completely explain the immune inflammatory response observed in ODE-exposed animals and cultured monocytes and macrophages (81). The predominance of gram-positive bacterial components, such as muramic acid, in addition to several elemental compounds, such as iron, was found to exist in the dust and likely skew the resultant inflammatory responses and phagocyte functionality (8, 81). Additionally, scant fungal and bacterial components in the dust may offset the immune paralysis caused by ACOD1; for example, β-glucan treatment has been found to inhibit LPS-induced ACOD1 expression and restore macrophage immune activity through the recovery of succinate dehydrogenase (SDH) expression (82). Alternative carbon sources capable of rescuing metabolic reprogramming or agents capable of modulating the inflammatory response are intrinsic to the complexity of the ODE exposure and likely account for the exposure-specific differences observed in our metabolomic studies.

TABLE 1 Phagocytic activity and reactive oxygen species (ROS) production of lung myeloid cell subpopulations at 48 h between WT and *Acod1*$^{-/-}$ mice following a one-time inhalant exposure to LPS.

	WT	*Acod1*$^{-/-}$
Neutrophils		
Phagocytic activity		
%BioParticle+	77.8 ± 0.886	74.6 ± 1.33
MFI	7,918 ± 259	7,783 ± 191
ROS		
%CellROX+	99.0 ± 0.0245	99.0 ± 0.0245
MFI	3,579 ± 429	3,403 ± 433
Activated macrophages		
Phagocytic activity		
%BioParticles+	81.7 ± 2.03	75.9 ± 2.58
MFI	11,521 ± 497	10,355 ± 830
ROS		
%CellROX+	99.0 ± 0.00	99.0 ± 0.00
MFI	6,193 ± 472	**8,035 ± 519***
Alveolar macrophages		
Phagocytic activity		
%BioParticles+	47.9 ± 4.07	43.6 ± 1.86
MFI	6,814 ± 409	7,501 ± 489
ROS		
%CellROX+	99.1 ± 0.0200	99.1 ± 0.0200
MFI	3,018 ± 932	3,607 ± 620
Monocytes–macrophages		
Phagocytic activity		
%BioParticles+	79.9 ± 1.56	75.7 ± 1.91
MFI	10,990 ± 453	9,943 ± 422
ROS		
%CellROX+	98.8 ± 0.132	99.0 ± 0.0200
MFI	3,466 ± 446	3,478 ± 577
Monocytes		
Phagocytic activity		
%BioParticles+	65.7 ± 1.45	59.2 ± 3.22
MFI	5,786 ± 257	5,264 ± 304
ROS		
%CellROX+	98.8 ± 0.186	99.0 ± 0.0200
MFI	3,870 ± 458	4,628 ± 505

Statistical difference vs. WT (*$p < 0.05$) (bold).
n = 5 (3 male and 2 female WT mice) and n = 5 (3 male and 2 female Acod1$^{-/-}$ mice).
MFI, mean fluorescence intensity.

ACOD1 was initially identified in 1995 as a bacterial LPS-inducible gene involved in innate immunity in mouse macrophages (83). Recently, cyclin-dependent kinase 2 (CDK2) was identified as a key regulator of ACOD1 expression in mouse and human monocytes and macrophages. CDK2 phosphorylation mediates the activation of mitogen-activated protein kinase 8 (MAPK8) which enables JUN-dependent transcription of *Acod1* (84). Although elucidation of the underlying mechanisms explains how inflammatory stimuli upregulate *Acod1* transcription and translation, recent advances in describing the dual role of the ACOD1–itaconate pathway in mediating inflammatory responses complicate its functional categorization. Currently, ACOD1 is considered as an immunometabolic regulator exerting a nuanced, context-dependent role where transcriptional activation of ACOD1 enables the catalysis of itaconate which can either directly or indirectly exert anti-inflammatory or proinflammatory effects (30). Preclinical studies using animal models of acute endotoxemia identified a protective effect of ACOD1 in mitigating lethal inflammation in sepsis, identifying the importance of ACOD1 expression in the antimicrobial armory of macrophages (31, 85). However, in a mouse study utilizing a cecal ligation-induced polymicrobial sepsis model, ACOD1 upregulation was responsible for the activation of immune pathways and sustained proinflammatory signaling through itaconate-dependent and independent mechanisms (84). The results of our current studies align with this latter study, where ACOD1 is important in facilitating a robust, proinflammatory response.

LPS- and ODE-induced upregulation of ACOD1 was associated with proinflammatory consequences induced with environmental exposure, and moreover, ACOD1 depletion resulted in protective benefits. Although the list of the known anti-inflammatory effects of ACOD1 is robust, knowledge related to the proinflammatory effects mediated by ACOD1 is rapidly expanding (30). For example, ACOD1 is capable of directly mediating ROS production which induces IL-1β, IL-6, IL-18, TNF, and CCL2 production (86). ACOD1 can also directly bind the GTPase, IMAP family member 7 (GIMAP7) and subsequently activate TNF pathways in isolation of itaconate production (84). Itaconate can inhibit aconitase 1 and 2 activity resulting in mitochondrial ROS (mROS) production and increased intracellular free iron, respectively (87). Both the resultant mROS and excess cellular iron-induced ROS production activate the NLRP3 inflammasome, which leads to CASP1-dependent IL-1β production (87). In contrast to our findings, others demonstrated that *Acod1*$^{-/-}$ animals had increased inflammatory/fibrotic consequences in a model of bleomycin-induced pulmonary fibrosis, suggesting that ACOD1 was important in limiting profibrotic and tissue remodeling processes (32). Intriguingly, in an LPS-induced endotoxemia model, induction of ACOD1 was found to reduce TNF production (88, 89), which also deviates from our findings in an inhaled exposure model. These diverging results support the dual nature of the ACOD1/itaconate immunometabolic axis and highlight the importance of the 1) nature of the primary niche interfacing with the exposure (systemic vs. tissue-targeted administration), 2) exposure duration (i.e., acute, repetitive,

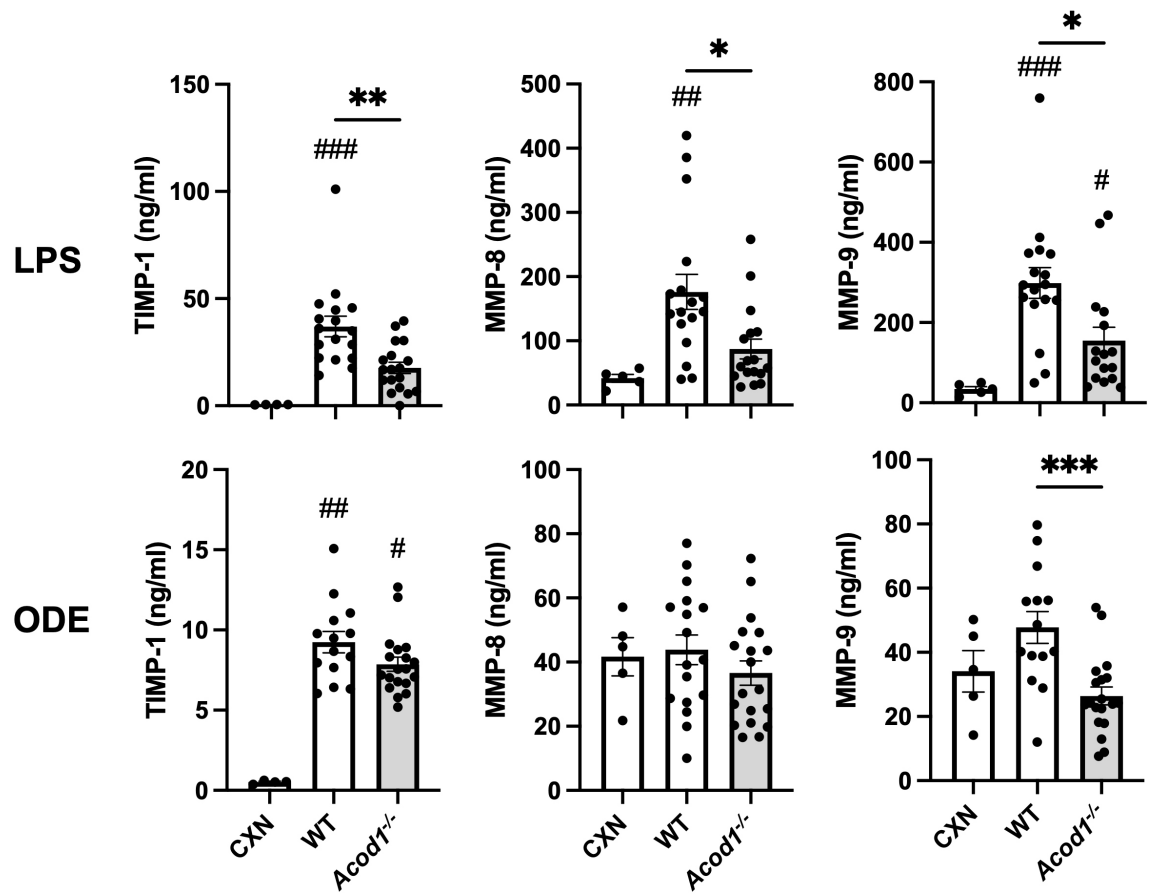

FIGURE 7
Mediators of tissue remodeling are decreased in *Acod1*$^{-/-}$ mice following environmental exposures. Scatter plot graphs depict the mean with SEM bars among treatment groups. Lung tissue levels of matrix metalloproteinases (MMPs) and tissue inhibitor of metalloproteinase (TIMP-1) are shown 48 h after a one-time LPS or ODE intratracheal instillation. n = 4–5 (CXN), n = 17 (7 male and 10 female WT mice exposed to LPS), n = 16–18 (6–8 male and 10 female *Acod1*$^{-/-}$ mice exposed to LPS), n = 17 (7 male and 10 female WT mice exposed to ODE), and n = 19 (9 male and 10 female *Acod1*$^{-/-}$ mice exposed to ODE). Statistical significance vs. CXN (#p < 0.05, ##p < 0.01, ###p < 0.001); between groups (*p < 0.05, **p < 0.01, ***p < 0.001).

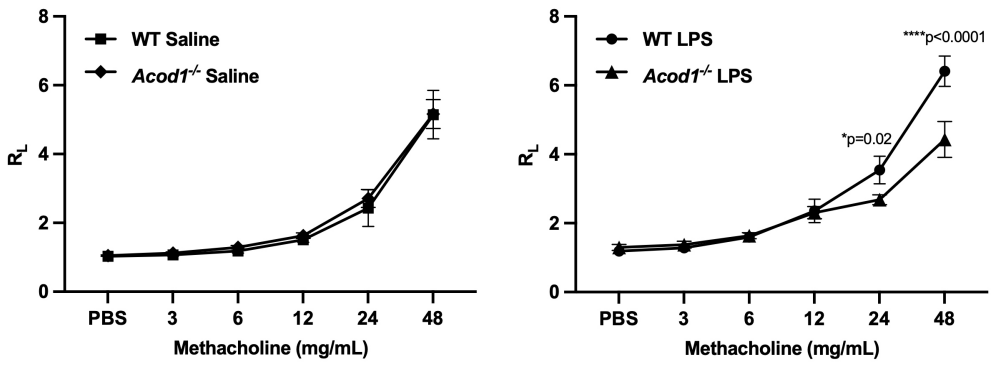

FIGURE 8
Acod1$^{-/-}$ mice demonstrated a blunted response to LPS-induced airway hyperresponsiveness (AHR). WT and *Acod1*$^{-/-}$ mice were initially treated with saline or LPS. Three hours following i.t. instillation, mice were tracheostomized and mechanically ventilated, and AHR to aerosolized methacholine (0 [PBS], 3, 6, 12, 24, 48 mg/mL) was measured and expressed as the mean (± SEM) total lung resistance (R_L). Statistical difference between the LPS and saline treatment groups was determined by repeated measures of a two-way ANOVA full fit model with a two-stage linear step-up procedure of Benjamini, Krieger, and Yekutieli to control for false discovery rate. n = 6 male mice/group.

time until euthanization post-exposure), and 3) exposure character (i.e., infectious, sterile, degree of complexity) when considering the role of ACOD1 in inflammation.

We performed functional assessments of myeloid-derived lung cells to ascertain whether the clearance ability of these innate immune cells was preserved or not in the absence of ACOD1 in the setting of LPS exposure. Our results demonstrated that *Acod1*$^{-/-}$ LPS-activated macrophages exhibited increased intracellular ROS with no other significant changes across myeloid populations regarding intracellular ROS production and phagocytic activity, indicating preservation of functional indices. LPS is known to polarize macrophages toward an M1-like phenotype which have characteristically high ROS (90). Itaconate, the bioactive metabolite of ACOD1, has been identified to limit M1 polarization in macrophages (91); therefore, our observation that *Acod1*$^{-/-}$ LPS-activated macrophages exhibited increased intracellular ROS is consistent with previous studies. However, it remains unknown whether ACOD1 impacts bacterial clearance in the setting of environmental exposures, an important area for future study. These future experiments will be complicated however, given multiple studies have demonstrated that the functionality (and relevance) of ACOD1 in infectious settings is specific to the bacterial species being studied. For example, myeloid cell-specific *Acod1* knockout mice are sensitive to *Mycobacterium tuberculosis* infection and have increased lung bacterial burden (92). *In-vitro* studies in *Acod1*-deficient bone marrow-derived macrophages also demonstrated enhanced replication of *Lactobacillus halophilus* (93). IFN-β or IFN-γ limits the intracellular growth of *Legionella pneumophila* by inducing the expression of ACOD1 and itaconate production *in vitro* and *in vivo* (93). Infection from *Salmonella* Typhimurium or *Mycobacterium avium* is also restricted by the induction of ACOD1 expression or itaconate production (31).

Although our study suggests a regulatory role for ACOD1 in environmental exposure-induced airway injury/inflammation, there are limitations. As this was an acute (one-time exposure) model of inflammatory agent-induced lung inflammation, we did not demonstrate consequences associated with chronic inflammatory lung disease, fibrosis development, or the associated fibrotic airway mechanics of changes in compliance and resistance. Future studies are warranted to investigate the role of ACOD1 in repeated environmental exposures. We also did not evaluate extrapulmonary organs (e.g., spleen, bone marrow, liver, kidney), apart from pulmonary draining lymph nodes, which may be necessary to clarify the systemic effect of ACOD1 in our animal model. There are also countless environmentally derived inflammatory agents in our exposome that could be responsible for adverse respiratory outcomes and should be explored including industrial chemicals (e.g., hydrogen sulfide, ammonia), heavy metals (e.g., cadmium, mercury), microbial agents (e.g., gram-positive peptidoglycan, fungal components), and other complex real-world exposures (e.g., burn pit exposures, air pollution, wildfire smoke).

In conclusion, ACOD1-deficient mice exhibited several decreased proinflammatory indicators, of those investigated, relative to ACOD1-sufficient mice. *Acod1* and proinflammatory transcripts (i.e., *Nos2*, *Ly6c1*) were also significantly upregulated in the murine monocyte/macrophage subpopulation representative of monocyte-derived macrophages (MDMs). Modulation of the ACOD1 immunometabolic axis could therefore prove beneficial via alteration of the MDM phenotype and function. Thus, future studies further characterizing the context-dependent regulatory effects of ACOD1 are necessary to optimally inform ACOD1/itaconate immunometabolic axis modulators to potentially elicit therapeutic benefit for at-risk persons.

Data availability statement

The datasets presented in this study can be found in online repositories. The names of the repository/repositories and accession number(s) can be found below: GSE267022 (GEO) and at https://doi.org/10.5281/zenodo.11060421 (Zenodo).

Ethics statement

Neither human participants, data, nor tissues were used in these experiments. The study was conducted and reported in accordance with ARRIVE guidelines (https://arriveguidelines.org). All animal procedures were approved by the University of Nebraska Medical Center (UNMC) Institutional Animal Care and Use Committee and were in accordance with NIH guidelines for the use of rodents.

Author contributions

AS: Conceptualization, Data curation, Formal analysis, Funding acquisition, Investigation, Methodology, Project administration, Resources, Software, Supervision, Validation, Visualization, Writing – original draft, Writing – review & editing. AN: Data curation, Investigation, Methodology, Resources, Writing – review & editing. AG: Data curation, Investigation, Methodology, Resources, Writing – review & editing. OS: Data curation, Investigation, Methodology, Resources, Writing – review & editing. TW: Data curation, Funding acquisition, Investigation, Methodology, Resources, Writing – review & editing. DS: Data curation, Formal analysis, Investigation, Methodology, Resources, Software, Writing – original draft, Writing – review & editing. PX: Data curation, Formal analysis, Investigation, Methodology, Resources, Software, Visualization, Writing – original draft, Writing – review & editing. VT: Data curation, Formal analysis, Investigation, Resources, Supervision, Writing – review & editing. CG: Data curation, Formal analysis, Investigation, Resources, Supervision, Writing – review & editing. KB: Conceptualization, Supervision, Writing – review & editing. TK: Conceptualization, Supervision, Writing – review & editing. GT: Conceptualization, Supervision, Writing – review & editing. JP: Conceptualization, Data curation, Formal analysis, Funding acquisition, Investigation, Methodology, Project administration, Resources, Software, Supervision, Validation, Visualization, Writing – original draft, Writing – review & editing.

Funding

The author(s) declare financial support was received for the research, authorship, and/or publication of this article. This study was funded by the National Institute for Occupational Safety and Health grant U54OH010162 (TW) and R01OH012045 (JAP), Department of Defense #PR200793 (JP). AS was supported by NIH grant 1F30ES036063-01 through the National Institute of Environmental Health Sciences (NIEHS). AS, TW, and JP received support from Central States Center of Agricultural Safety and Health (CS-CASH). TW is supported by grants from the VA (BLR&D Merit I01 BX005886) and National Institutes of Health (P50 AA030407). TW is the recipient of a Research Career Scientist Award (IK6 BX005962) from the Department of Veterans Affairs. VCT (Metabolomics Core) was supported by NIH grant P01A1083211 through the National Institute of Allergy and Infectious Disease (NIAID).

Acknowledgments

The authors acknowledge Craig Semerad, Victoria B. Smith, and Holly Britton in the Flow Cytometry Research Core Facility at the University of Nebraska Medical Center for aiding with the flow cytometry studies. This core facility is administrated through the Office of the Vice Chancellor for Research and supported by state funds from the Nebraska Research Initiative (NRI) and The Fred and Pamela Buffett Cancer Center's National Cancer Institute Cancer Support Grant. Major instrumentation has been provided by the Office of the Vice Chancellor for Research, The University of Nebraska Foundation, the Nebraska Banker's Fund, and by the NIH-NCRR Shared Instrument Program. The University of Nebraska DNA Sequencing Core and the Bioinformatics and Systems Biology Core received partial support from the National Institute for General Medical Science (NIGMS) INBRE - P20GM103427-19 grant as well as The Fred & Pamela Buffett Cancer Center Support Grant - P30 CA036727. This publication's contents are the sole responsibility of the authors and do not necessarily represent the official views of the NIH or NIGMS.

Conflict of interest

JP has received research reagent from AstraZeneca (no monies) and has been a site investigator for allergy and asthma clinical studies for Takeda, GlaxoSmithKline, Regeneron, Areteia, and AstraZeneca (no monies).

The remaining authors declare that the research was conducted in the absence of any commercial or financial relationships that could be construed as a potential conflict of interest.

Publisher's note

Supplementary material

The Supplementary Material for this article can be found online at: https://www.frontiersin.org/articles/10.3389/fimmu.2024.1432334/full#supplementary-material

SUPPLEMENTARY FIGURE 1
Gating strategy for identification of non-debris, singlets, live CD45+ myeloid and lymphoid cells. For flow analysis, all panels were first gated as forward scatter-area (FSC-A) x side scatter-area (SSC-A) to omit debris, dead and/or apoptotic cells. This was followed by two single cell gates to omit doublets (FSC-A x FSC-height (H) and SSC-A x SSC-H), followed by a live/dead gate and then a CD45 gate to ensure removal of any additional dead or apoptotic cells and non-leukocytes. The $CD45^+$ cells were gated on CD11c x Ly6G to select $Ly6G^+$ neutrophils. Non-neutrophils were gated for B cells (CD19 x SSC gate). This was followed by non-B cells gated on CD11c x CD11b to select $CD11c^+CD11b^{lo}$ alveolar (Alv) macrophages (Mϕ), $CD11c^+CD11b^{hi}$ activated (Act) Mϕ, $CD11c^{int}CD11b^{hi}$ transitioning monocytes (Mono)-Mϕ, and $CD11c^-CD11b^{hi}$ monocytes (Mono). The negative or non-monocyte/macrophage populations were gated on CD3 x NK1.1 to select $CD3^+$ T cells and $CD3^-NK1.1^+$ NK cells, and then a CD4 x CD8 gate to select $CD3^+CD4^+$ and $CD3^+CD8^+$ T cells.

SUPPLEMENTARY FIGURE 2
Gating strategy for characterization of pulmonary draining lymph node cellular composition. For flow analysis, all panels were first gated as forward scatter-area (FSC-A) x side scatter-area (SSC-A) to omit debris, dead and/or apoptotic cells. This was followed by two single cell gates to omit doublets (FSC-A x FSC-height (H) and SSC-A x SSC-H), followed by a live/dead gate and then a CD45 gate to ensure removal of any additional dead or apoptotic cells and non-leukocytes. The CD45+ cells were gated on CD11c x Ly6G to select Ly6G+ neutrophils. Non-neutrophils were gated for B cells (CD19 x SSC gate). This was followed by non-B cells gated on CD3 x CD24 to identify dendritic cells. Non-dendritic cells were gated for monocytes by selecting cells doubly positive for Ly6C x CD11b. Non-monocytes were then gated to distinguish macrophages ($CD11c^+CD11b^{variable}$). The negative gate that includes non-macrophages was gated by CD3 x NK1.1 to select $CD3^+$ T cells and $CD3^-NK1.1^+$ NK cells, and then a CD4 x CD8 gate to select $CD3^+CD4^+$ and $CD3^+CD8^+$ T cells.

SUPPLEMENTARY FIGURE 3
Acod1$^{-/-}$ mice do not exhibit differences in LPS or ODE-induced lung inflammation or collagen 48 hours post-treatment. **(A)** Representative images from treatment groups stained by H&E. **(B)** Scatter plots with bars depict mean with SEM of semi-quantitative lung inflammatory score for each mouse. n=5 (CXN), n=19 (9 male and 10 female WT mice, LPS), n=18 (8 male and 10 female *Acod1*$^{-/-}$ mice, LPS), n=17 (7 male and 10 female WT mice, ODE), and n=19 (9 male and 10 female *Acod1*$^{-/-}$ mice, ODE). **(C)** Representative images from treatment groups stained by trichrome. **(D)** Scatter plot with bars depicts mean with SEM of integrate density of collagen quantified per each mouse. n=3 (CXN), n=6 (3 male and 3 female WT mice, LPS), n=5 (2 male and 3 female *Acod1*$^{-/-}$ mice, LPS), n=5 (2 male and 3 female WT mice, ODE), and n=6 (3 male and 3 female *Acod1*$^{-/-}$ mice, ODE). Statistical significance vs. CXN (##p<0.01).

References

1. Prüss-Ustün A, Wolf J, Corvalán C, Neville T, Bos R, Neira M, et al. Diseases due to unhealthy environments: an updated estimate of the global burden of disease attributable to environmental determinants of health. *J Public Health (Oxf)*. (2017) 39:464–75. doi: 10.1093/pubmed/fdw085

2. Rolph CA, Gwyther CL, Tyrrel SF, Nasir ZA, Drew GH, Jackson SK, et al. Sources of airborne endotoxins in ambient air and exposure of nearby communities—A review. *Atmosphere*. (2018) 9:375. doi: 10.3390/atmos9100375

3. Tager IB, Lurmann FW, Haght T, Alcorn S, Penfold B, Hammond SK. Temporal and spatial patterns of ambient endotoxin concentrations in Fresno, California. *Environ Health Perspect*. (2010) 118:1490–6. doi: 10.1289/ehp.0901602

4. Park S, Allen RJ, Lim CH. A likely increase in fine particulate matter and premature mortality under future climate change. *Air Quality Atmosphere Health*. (2020) 13:143–51. doi: 10.1007/s11869-019-00785-7

5. Joshi M, Goraya H, Joshi A, Bartter T. Climate change and respiratory diseases: a 2020 perspective. *Curr Opin Pulm Med*. (2020) 26:119–27. doi: 10.1097/MCP.0000000000000656

6. De Matteis S, Heederik D, Burdorf A, Colosio C, Cullinan P, Henneberger PK, et al. Current and new challenges in occupational lung diseases. *Eur Respir Rev*. (2017) 26. doi: 10.1183/16000617.0080-2017

7. Farokhi A, Heederik D, Smit LAM. Respiratory health effects of exposure to low levels of airborne endotoxin - a systematic review. *Environ Health*. (2018) 17:14. doi: 10.1186/s12940-018-0360-7

8. Boissy RJ, Romberger DJ, Roughead WA, Weissenburger-Moser L, Poole JA, LeVan TD. Shotgun pyrosequencing metagenomic analyses of dusts from swine confinement and grain facilities. *PLoS One*. (2014) 9:e95578. doi: 10.1371/journal.pone.0095578

9. Basinas I, Sigsgaard T, Kromhout H, Heederik D, Wouters IM, Schlunssen V. A comprehensive review of levels and determinants of personal exposure to dust and endotoxin in livestock farming. *J Expo Sci Environ Epidemiol*. (2015) 25:123–37. doi: 10.1038/jes.2013.83

10. Moller W, Heimbeck I, Hofer TP, Khadem Saba G, Neiswirth M, Frankenberger, M, et al. Differential inflammatory response to inhaled lipopolysaccharide targeted either to the airways or the alveoli in man. *PLoS One*. (2012) 7:e33505. doi: 10.1371/journal.pone.0033505

11. Misharin AV, Morales-Nebreda L, Reyfman PA, Cuda CM, Walter JM, McQuattie-Pimentel AC, et al. Monocyte-derived alveolar macrophages drive lung fibrosis and persist in the lung over the life span. *J Exp Med*. (2017) 214:2387–404. doi: 10.1084/jem.20162152

12. Lin CK, Huang TH, Yang CT, Shi CS. Roles of lung-recruited monocytes and pulmonary Vascular Endothelial Growth Factor (VEGF) in resolving Ventilator-Induced Lung Injury (VILI). *PLoS One*. (2021) 16:e0248959. doi: 10.1371/journal.pone.0248959

13. Hu G, Christman JW. Editorial: alveolar macrophages in lung inflammation and resolution. *Front Immunol*. (2019) 10:2275. doi: 10.3389/fimmu.2019.02275

14. Morales-Nebreda L, Misharin AV, Perlman H, Budinger GR. The heterogeneity of lung macrophages in the susceptibility to disease. *Eur Respir Rev*. (2015) 24:505–9. doi: 10.1183/16000617.0031-2015

15. Poole JA, Gaurav R, Schwab A, Nelson AJ, Gleason A, Romberger DJ, et al. Post-endotoxin exposure-induced lung inflammation and resolution consequences beneficially impacted by lung-delivered IL-10 therapy. *Sci Rep*. (2022) 12:17338. doi: 10.1038/s41598-022-22346-2

16. Yamasaki K, Eeden SFV. Lung macrophage phenotypes and functional responses: role in the pathogenesis of COPD. *Int J Mol Sci*. (2018) 19. doi: 10.3390/ijms19020582

17. Poole JA, Dooley GP, Saito R, Burrell AM, Bailey KL, Romberger DJ, et al. Muramic acid, endotoxin, 3-hydroxy fatty acids, and ergosterol content explain monocyte and epithelial cell inflammatory responses to agricultural dusts. *J Toxicol Environ Health A*. (2010) 73:684–700. doi: 10.1080/15287390903578539

18. Schwab AD, Wyatt TA, Nelson AJ, Gleason A, Gaurav R, Romberger DJ, et al. Lung-delivered IL-10 therapy elicits beneficial effects via immune modulation in organic dust exposure-induced lung inflammation. *J Immunotoxicol*. (2024) 21:2332172. doi: 10.1080/1547691X.2024.2332172

19. Schwab AD, Wyatt TA, Moravec G, Thiele GM, Nelson AJ, Gleason A, et al. Targeting transitioning lung monocytes/macrophages as treatment strategies in lung disease related to environmental exposures. *Respir Res*. (2024) 25:157. doi: 10.1186/s12931-024-02804-3

20. Long H, Lichtnekert J, Andrassy J, Schraml BU, Romagnani P, Anders HJ. Macrophages and fibrosis: how resident and infiltrating mononuclear phagocytes account for organ injury, regeneration or atrophy. *Front Immunol*. (2023) 14:1194988. doi: 10.3389/fimmu.2023.1194988

21. Perrot CY, Karampitsakos T, Herazo-Maya JD. Monocytes and macrophages: emerging mechanisms and novel therapeutic targets in pulmonary fibrosis. *Am J Physiol Cell Physiol*. (2023) 325:C1046–57. doi: 10.1152/ajpcell.00302.2023

22. Russell DG, Huang L, VanderVen BC. Immunometabolism at the interface between macrophages and pathogens. *Nat Rev Immunol*. (2019) 19:291–304. doi: 10.1038/s41577-019-0124-9

23. Liu Q, Tian X, Maruyama D, Arjomandi M, Prakash A. Lung immune tone via gut-lung axis: gut-derived LPS and short-chain fatty acids' immunometabolic regulation of lung IL-1beta, FFAR2, and FFAR3 expression. *Am J Physiol Lung Cell Mol Physiol*. (2021) 321:L65–78. doi: 10.1152/ajplung.00421.2020

24. O'Beirne SL, Kikkers SA, Oromendia C, Salit J, Rostmai MR, Ballman KV, et al. Alveolar macrophage immunometabolism and lung function impairment in smoking and chronic obstructive pulmonary disease. *Am J Respir Crit Care Med*. (2020) 201:735–9. doi: 10.1164/rccm.201908-1683LE

25. Tomlinson KL, Prince AS, Wong Fok Lung T. Immunometabolites drive bacterial adaptation to the airway. *Front Immunol*. (2021) 12:790574. doi: 10.3389/fimmu.2021.790574

26. Van den Bossche J, O'Neill LA, Menon D. Macrophage immunometabolism: where are we (Going)? *Trends Immunol*. (2017) 38:395–406. doi: 10.1016/j.it.2017.03.001

27. Kolliniati O, Ieronymaki E, Vergadi E, Tsatsanis C. Metabolic regulation of macrophage activation. *J Innate Immun*. (2022) 14:51–68. doi: 10.1159/000516780

28. Hall CJ, Boyle RH, Astin JW, Flores MV, Oehlers SH, Sanderson LE, et al. Immunoresponsive gene 1 augments bactericidal activity of macrophage-lineage cells by regulating beta-oxidation-dependent mitochondrial ROS production. *Cell Metab*. (2013) 18:265–78. doi: 10.1016/j.cmet.2013.06.018

29. Wu R, Chen F, Wang N, Tang D, Kang R. ACOD1 in immunometabolism and disease. *Cell Mol Immunol*. (2020) 17:822–33. doi: 10.1038/s41423-020-0489-5

30. Wu R, Liu J, Tang D, Kang R. The dual role of ACOD1 in inflammation. *J Immunol*. (2023) 211:518–26. doi: 10.4049/jimmunol.2300101

31. Wu R, Kang R, Tang D. Mitochondrial ACOD1/IRG1 in infection and sterile inflammation. *J Intensive Med*. (2022) 2:78–88. doi: 10.1016/j.jointm.2022.01.001

32. Ogger PP, Albers GJ, Hewitt RJ, O'Sullivan BJ, Powell JE, Calamita E, et al. Itaconate controls the severity of pulmonary fibrosis. *Sci Immunol*. (2020) 5. doi: 10.1126/sciimmunol.abc1884

33. Demars A, Vitali A, Comein A, Carlier E, Azouz A, Goriely S, et al. Aconitate decarboxylase 1 participates in the control of pulmonary Brucella infection in mice. *PLoS Pathog*. (2021) 17:e1009887. doi: 10.1371/journal.ppat.1009887

34. Sohail A, Iqbal AA, Sahini N, Chen F, Tantawy M, Waqas SFH, et al. Correction: Itaconate and derivatives reduce interferon responses and inflammation in influenza A virus infection. *PLoS Pathog*. (2022) 18:e1011002. doi: 10.1371/journal.ppat.1011002

35. Qui JH, Zhang L, Li KX, Zhang QH, Fan KR, Chen K, et al. Deficiency of IRG1/itaconate aggravates endotoxemia-induced acute lung injury by inhibiting autophagy in mice. *Exp Anim*. (2023) 72:164–72. doi: 10.1538/expanim.22-0104

36. Sun KA, Li Y, Meliton AY, Woods PS, Kimmig LM, Cetin-Atalay R, et al. Endogenous itaconate is not required for particulate matter-induced NRF2 expression or inflammatory response. *Elife*. (2020) 9. doi: 10.7554/eLife.54877

37. Guan M, Yao J, Wang Y, Fang S, Hu Y, Wang A, et al. Airborne endotoxin in fine particulate matter in Beijing. *Atmospheric Environ*. (2014) 97:35–42. doi: 10.1016/j.atmosenv.2014.08.005

38. Ko G, Simmons IIIOD, Likirdopulos CA, Worley-Davis L, Williams CM, Sobsey MD. Endotoxin levels at swine farms using different waste treatment and management technologies. *Environ Sci Technol*. (2010) 44:3442–8. doi: 10.1021/es9026024

39. Nelson AJ, Roy SK, Warren K, Janike K, Thiele GM, Mikuls TR, et al. Sex differences impact the lung-bone inflammatory response to repetitive inhalant lipopolysaccharide exposures in mice. *J Immunotoxicol*. (2018) 15:73–81. doi: 10.1080/1547691X.2018.1460425

40. Redente EF, Keith RC, Janssen W, Henson PM, Ortiz LA, Downey GP, et al. Tumor necrosis factor-alpha accelerates the resolution of established pulmonary fibrosis in mice by targeting profibrotic lung macrophages. *Am J Respir Cell Mol Biol*. (2014) 50:825–37. doi: 10.1165/rcmb.2013-0386OC

41. Poole JA, Nordgren TM, Heires AJ, Nelson AJ, Katafiasz D, Bailey KL, et al. Amphiregulin modulates murine lung recovery and fibroblast function following exposure to agriculture organic dust. *Am J Physiol Lung Cell Mol Physiol*. (2020) 318:L180–91. doi: 10.1152/ajplung.00039.2019

42. Kirby AC, Raynes JG, Kaye PM. CD11b regulates recruitment of alveolar macrophages but not pulmonary dendritic cells after pneumococcal challenge. *J Infect Dis*. (2006) 193:205–13. doi: 10.1086/498874

43. Lee J, Boyce S, Powers J, Baer C, Sassetti CM, Behar SM. CD11cHi monocyte-derived macrophages are a major cellular compartment infected by Mycobacterium tuberculosis. *PLoS Pathog*. (2020) 16:e1008621. doi: 10.1371/journal.ppat.1008621

44. Andrews S. FastQC: A quality control tool for high throughput sequence data (2010). Available online at: http://www.bioinformatics.babraham.ac.uk/projects/fastqc/. (Accessed August 1, 2022).

45. Dobin A, Davis CA, Schlesinger F, Drenkow J, Zaleski C, Jha S, et al. STAR: ultrafast universal RNA-seq aligner. *Bioinformatics*. (2013) 29:15–21. doi: 10.1093/bioinformatics/bts635

46. Li B, Dewey CN. RSEM: accurate transcript quantification from RNA-Seq data with or without a reference genome. *BMC Bioinf*. (2011) 12:323. doi: 10.1186/1471-2105-12-323

47. Love MI, Huber W, Anders S. Moderated estimation of fold change and dispersion for RNA-seq data with DESeq2. *Genome Biol*. (2014) 15:550. doi: 10.1186/s13059-014-0550-8

48. Benjamini Y, Hochberg Y. Controlling the false discovery rate: A practical and powerful approach to multiple testing. *J R Stat Society Ser B (Methodological)*. (1995) 57:289–300. doi: 10.1111/j.2517-6161.1995.tb02031.x

49. Poole JA, Thiele GM, Janike K, Nelson AJ, Duryee MJ, Rentfro K, et al. Combined collagen-induced arthritis and organic dust-induced airway inflammation to model inflammatory lung disease in rheumatoid arthritis. *J Bone Miner Res*. (2019) 34:1733–43. doi: 10.1002/jbmr.3745

50. Rayamajhi M, Redente EF, Condon TV, Gonzalez-Juarrero M, Riches FW, Lenz LL. Non-surgical intratracheal instillation of mice with analysis of lungs and lung draining lymph nodes by flow cytometry. *J Vis Exp*. (2011). doi: 10.3791/2702

51. Poole JA, Gleason AM, Bauer C, West WW, Alexis N, van Rooijen N, et al. CD11c (+)/CD11b(+) cells are critical for organic dust-elicited murine lung inflammation. *Am J Respir Cell Mol Biol*. (2012) 47:652–9. doi: 10.1165/rcmb.2012-0095OC

52. Poole JA, Mikuls TR, Duryee MJ, Warren KJ, Wyatt TA, Nelson AJ, et al. A role for B cells in organic dust induced lung inflammation. *Respir Res*. (2017) 18:214. doi: 10.1186/s12931-017-0703-x

53. Robbe P, Draijer C, Borg TR, Luinge M, Timens W, Wouters IM, et al. Distinct macrophage phenotypes in allergic and nonallergic lung inflammation. *Am J Physiol Lung Cell Mol Physiol*. (2015) 308:L358–367. doi: 10.1152/ajplung.00341.2014

54. Mikuls TR, Gaurav R, Thiele GM, England BR, Wolfe MG, Shaw BP, et al. The impact of airborne endotoxin exposure on rheumatoid arthritis-related joint damage, autoantigen expression, autoimmunity, and lung disease. *Int Immunopharmacol*. (2021) 100:108069. doi: 10.1016/j.intimp.2021.108069

55. Tacconi C, Commerford CD, Dieterich LC, Schwager S, He Y, Ikenberg K, et al. CD169(+) lymph node macrophages have protective functions in mouse breast cancer metastasis. *Cell Rep*. (2021) 35:108993. doi: 10.1016/j.celrep.2021.108993

56. Hornsteiner F, Sykora MM, Tripp CH, Sopper S, Stoitzner P. Mouse dendritic cells and other myeloid subtypes in healthy lymph nodes and skin: 26-Color flow cytometry panel for immune phenotyping. *Eur J Immunol*. (2022) 52:2006–9. doi: 10.1002/eji.202250004

57. Zhang X, Yu C, Liu JQ, Bai XF. Dendritic cell expression of CD24 contributes to optimal priming of T lymphocytes in lymph nodes. *Front Immunol*. (2023) 14:1116749. doi: 10.3389/fimmu.2023.1116749

58. Wyatt TA, Nemecek M, Chandra D, DeVasure JM, Nelson AJ, Romberger DJ, et al. Organic dust-induced lung injury and repair: Bi-directional regulation by TNFalpha and IL-10. *J Immunotoxicol*. (2020) 17:153–62. doi: 10.1080/1547691X.2020.1776428

59. Landini G, Martinelli G, Piccinini F. Colour deconvolution: stain unmixing in histological imaging. *Bioinformatics*. (2021) 37:1485–7. doi: 10.1093/bioinformatics/btaa847

60. Hakansson HF, Smailagic A, Brunmark C, Miller-Larsson A, Lal H. Altered lung function relates to inflammation in an acute LPS mouse model. *Pulm Pharmacol Ther*. (2012) 25:399–406. doi: 10.1016/j.pupt.2012.08.001

61. Albright M, Guttenberg MA, Tighe RM. Ozone-induced models of airway hyperreactivity and epithelial injury. *Methods Mol Biol*. (2022) 2506:67–81. doi: 10.1007/978-1-0716-2364-0_5

62. Sundblad BM, von Scheele I, Palmberg L, Olsson M, Larsson K. Repeated exposure to organic material alters inflammatory and physiological airway responses. *Eur Respir J*. (2009) 34:80–8. doi: 10.1183/09031936.00105308

63. Hollingsworth JW 2nd, Cook DN, Brass DM, Walker JK, Morgan DL, Foster WM, et al. The role of Toll-like receptor 4 in environmental airway injury in mice. *Am J Respir Crit Care Med*. (2004) 170:126–32. doi: 10.1164/rccm.200311-1499OC

64. Schwartz DA, Christ WJ, Kleeberger SR, Wohlford-Lenane CL. Inhibition of LPS-induced airway hyperresponsiveness and airway inflammation by LPS antagonists. *Am J Physiol Lung Cell Mol Physiol*. (2001) 280:L771–778. doi: 10.1152/ajplung.2001.280.4.L771

65. Poole JA, Wyath TA, Oldenburg PJ, Elliott MK, West WW, Sisson JH, et al. Intranasal organic dust exposure-induced airway adaptation response marked by persistent lung inflammation and pathology in mice. *Am J Physiol Lung Cell Mol Physiol*. (2009) 296:L1085–1095. doi: 10.1152/ajplung.90622.2008

66. Seifert SA, Von Essen S, Jacobitz K, Crouch R, Lintner CP. Organic dust toxic syndrome: a review. *J Toxicol Clin Toxicol*. (2003) 41:185–93. doi: 10.1081/clt-120019136

67. Bain CC, MacDonald AS. The impact of the lung environment on macrophage development, activation and function: diversity in the face of adversity. *Mucosal Immunol*. (2022) 15:223–34. doi: 10.1038/s41385-021-00480-w

68. Du Clos TW. Pentraxins: structure, function, and role in inflammation. *ISRN Inflammation*. (2013) 2013:379040. doi: 10.1155/2013/379040

69. Davey A, McAuley DF, O'Kane CM. Matrix metalloproteinases in acute lung injury: mediators of injury and drivers of repair. *Eur Respir J*. (2011) 38:959–70. doi: 10.1183/09031936.00032111

70. Bauer C, Kielian T, Wyatt TA, Romberger DJ, West WW, Gleason AM, et al. Myeloid differentiation factor 88-dependent signaling is critical for acute organic dust-induced airway inflammation in mice. *Am J Respir Cell Mol Biol*. (2013) 48:781–9. doi: 10.1165/rcmb.2012-0479OC

71. Pandher U, Kirychuk S, Schneberger D, Thompson B, Aulakh G, Sethi RS, et al. Pulmonary inflammatory response from co-exposure to LPS and glyphosate. *Environ Toxicol Pharmacol*. (2021) 86:103651. doi: 10.1016/j.etap.2021.103651

72. Brass DM, Hollingsworth JW, Cinque M, Li Z, Potts E, Toloza E, et al. Chronic LPS inhalation causes emphysema-like changes in mouse lung that are associated with apoptosis. *Am J Respir Cell Mol Biol*. (2008) 39:584–90. doi: 10.1165/rcmb.2007-0448OC

73. Laskin DL, Malaviya R, Laskin JD. Role of macrophages in acute lung injury and chronic fibrosis induced by pulmonary toxicants. *Toxicol Sci*. (2019) 168:287–301. doi: 10.1093/toxsci/kfy309

74. Oliveira VLS, Pollenus E, Berghmans N, Queiroz-Junior CM, Blanter M, Mattos MS, et al. Absence of CCR2 promotes proliferation of alveolar macrophages that control lung inflammation in acute respiratory distress syndrome in mice. *Int J Mol Sci*. (2022) 23. doi: 10.3390/ijms232112920

75. Zeng Z, Lan T, Wei Y, Wei X. CCL5/CCR5 axis in human diseases and related treatments. *Genes Dis*. (2022) 9:12–27. doi: 10.1016/j.gendis.2021.08.004

76. Castanheira F, de Lima KA, Cebinelli GCM, Sonego F, Kanashiro A, Colon DF, et al. CCR5-positive inflammatory monocytes are crucial for control of sepsis. *Shock*. (2019) 52:e100–6. doi: 10.1097/SHK.0000000000001301

77. Lin J, Xu Y, Guo P, Chen YJ, Zhou J, Xia M, et al. CCL5/CCR5-mediated peripheral inflammation exacerbates blood–brain barrier disruption after intracerebral hemorrhage in mice. *J Transl Med*. (2023) 21:196. doi: 10.1186/s12967-023-04044-3

78. Rosanna DP, Salvatore C. Reactive oxygen species, inflammation, and lung diseases. *Curr Pharm Des*. (2012) 18:3889–900. doi: 10.2174/138161212802083716

79. Guo C, Atochina-Vasserman E, Abramova H, George B, Manoj V, Scott P, et al. Role of NOS2 in pulmonary injury and repair in response to bleomycin. *Free Radic Biol Med*. (2016) 91:293–301. doi: 10.1016/j.freeradbiomed.2015.10.417

80. Li YH, Zhang Y, Pan G, Xiang LX, Luo DC, Shao JZ. Occurrences and functions of ly6C(hi) and ly6C(lo) macrophages in health and disease. *Front Immunol*. (2022) 13:901672. doi: 10.3389/fimmu.2022.901672

81. Poole JA, Alexis NE, Parks C, MacInnes AK, Gentry-Nielsen MJ, Fey PD, et al. Repetitive organic dust exposure *in vitro* impairs macrophage differentiation and function. *J Allergy Clin Immunol*. (2008) 122:375–382, 382.e371-374. doi: 10.1016/j.jaci.2008.05.023

82. Dominguez-Andres J, Novakovic B, Li Y, Scicluna BP, Gresnigt MS, Arts RJW, et al. The itaconate pathway is a central regulatory node linking innate immune tolerance and trained immunity. *Cell Metab*. (2019) 29:211–220.e215. doi: 10.1016/j.cmet.2018.09.003

83. Lee CG, Jenkins NA, Gilbert DJ, Copeland NG, O'Brien WE. Cloning and analysis of gene regulation of a novel LPS-inducible cDNA. *Immunogenetics*. (1995) 41:263–70. doi: 10.1007/BF00172150

84. Wu R, Liu J, Wang N, Zeng L, Yu C, Chen F, et al. Aconitate decarboxylase 1 is a mediator of polymicrobial sepsis. *Sci Transl Med*. (2022) 14:eabo2028. doi: 10.1126/scitranslmed.abo2028

85. Michelucci A, Cordes T, Ghelfi J, Pailot A, Reiling N, Goldmann O, et al. Immune-responsive gene 1 protein links metabolism to immunity by catalyzing itaconic acid production. *Proc Natl Acad Sci U.S.A*. (2013) 110:7820–5. doi: 10.1073/pnas.1218599110

86. Ren K, Lv Y, Zhou Y, Chen C, Shi H, Guo L, et al. Suppression of IRG-1 reduces inflammatory cell infiltration and lung injury in respiratory syncytial virus infection by reducing production of reactive oxygen species. *J Virol*. (2016) 90:7313–22. doi: 10.1128/JVI.00563-16

87. Liu X, Shi B, Suo R, Xiong S, Wang X, Liang X, et al. Itaconate regulates macrophage function through stressful iron-sulfur cluster disrupting and iron metabolism rebalancing. *FASEB J*. (2021) 35:e21936. doi: 10.1096/fj.202100726RR

88. Jamal Uddin M, Joe Y, Kim SK, Oh Jeong S, Ryter SW, Pae HO, et al. IRG1 induced by heme oxygenase-1/carbon monoxide inhibits LPS-mediated sepsis and pro-inflammatory cytokine production. *Cell Mol Immunol*. (2016) 13:170–9. doi: 10.1038/cmi.2015.02

89. Mills EL, Ryan DG, Prag HA, Dikovskaya D, Menon D, Zaslona Z, et al. Itaconate is an anti-inflammatory metabolite that activates Nrf2 via alkylation of KEAP1. *Nature*. (2018) 556:113–7. doi: 10.1038/nature25986

90. Yang Y, Wang Y, Guo L, Gao W, Tang TL, Yan M, et al. Interaction between macrophages and ferroptosis. *Cell Death Dis*. (2022) 13:355. doi: 10.1038/s41419-022-04775-z

91. Lang R, Siddique M. Control of immune cell signaling by the immuno-metabolite itaconate. *Front Immunol*. (2024) 15:1352165. doi: 10.3389/fimmu.2024.1352165

92. Nair S, Huynh JP, Lampropoulou V, Loginicheva E, Esaulova E, Gounder AP, et al. Irg1 expression in myeloid cells prevents immunopathology during M. tuberculosis infection. *J Exp Med*. (2018) 215:1035–45. doi: 10.1084/jem.20180118

93. Naujoks J, Tabeling C, Dill BD, Hoffmann C, Brown AS, Kunze M, et al. IFNs modify the proteome of legionella-containing vacuoles and restrict infection via IRG1-derived itaconic acid. *PLoS Pathog*. (2016) 12:e1005408. doi: 10.1371/journal.ppat.1005408